Rezgui, D., & Lowenberg, M. H. (2020). Nonlinear Blade Stability for a Scaled Autogyro Rotor at High Advance Ratios. *Journal of the American Helicopter Society*, *65*(1), 1-19. https://doi.org/10.4050/JAHS.65.012005

Nonlinear Blade Stability for a Scaled Autogyro Rotor at High Advance Ratios

Djamel Rezgui[1]

Lecturer in Aerospace Engineering,

University of Bristol,

Bristol, UK

Mark H. Lowenberg[2]

Professor of Flight Dynamics,

University of Bristol,

Bristol, UK

Abstract

Despite current research advances in aircraft dynamics and increased interest in the slowed rotor concept for high speed compound helicopters, the stability of autogyro rotors remains partially understood, particularly at lightly-loaded conditions and high advance ratios. In autorotation, the periodic behavior of a rotor blade is a complex nonlinear phenomenon, further complicated by the fact that the rotor speed is not held constant. The aim of the analysis presented in this article is to investigate the underlying mechanisms that can lead to rotation-flap blade instability at high advance ratios for a teetering autorotating rotor. The stability analysis was conducted via wind tunnel tests of a scaled autogyro model combined with numerical continuation and bifurcation analysis. The investigation assessed the effect of varying the flow speed, blade pitch angle and rotor shaft tilt relative to the flow, on the rotor performance and blade stability. The results revealed that rotor instability

[1]Lecturer in Aerospace Engineering, Department of Aerospace Engineering, Bristol, UK

[2]Professor of Flight Dynamics, Department of Aerospace Engineering, Bristol, UK

in autorotation is associated with the existence of fold bifurcations, which bound the control-input and design parameter space within which the rotor can autorotate. This instability occurs at a lightly loaded condition and at advance ratios close to 1 for the scaled model. Finally, it was also revealed that the rotor inability to autorotate was driven by blade stall.

Nomenclature

$\dot{()}$	derivative with respect to time
$a_{hub,i}^{shaft}$	translational acceleration vectors of the hub in the shaft axes respectively
C_d, C_l	two-dimensional drag and lift coefficients
D, L	drag and lift aerodynamic force components
f	generic function
I_{blade}	blade second moment of inertia
L_{aero}, M_{aero}	aerodynamic rolling and pitching moments respectively in the wind axes
$M_{aero,i}, N_{aero,i}$	aerodynamic flapping moment and torque respectively for blade i
$M_{\beta,i}, N_{\psi,i}$	total flapping moment and torque respectively acting on blade i
M_{blade}	blade mass moment
$P_i^{shaft}, Q_i^{shaft}, R_i^{shaft}$	angular velocities of the rotor hub in the shaft axes
p	parameter vector
R	blade tip radius
r	elemental blade radial position
T_{aero}	rotor thrust
U	forward flow speed
$u_{hub}, v_{hub}, w_{hub}$	flow velocity components relative to the rotor hub
x	state vector
α	local angle of attack
$\alpha_{hub,i}^{shaft}$	angular acceleration vector of the hub in the shaft axes
α_{hub}^{disc}	angular acceleration vector of the hub in the rotor disc axes

β	blade flapping angle
ζ	friction coefficient
θ	local blade pitch angle
θ_{col}	blade collective pitch angle
θ_{shaft}	rotor shaft tilt angle
ν_i	induced velocity at the i^{th} blade element
$\nu_{i,m}$	the induced velocity from momentum theory
ν_0, ν_s, ν_c	average, lateral and longitudinal induced velocity components
ϕ	local inflow angle
χ	rotor wake skew angle
ψ	blade azimuthal position
Ω	rotor speed

Introduction

Unlike the helicopter, the autogyro produces lift in forward flight by relying on the phenomenon of autorotation to maintain rotor spinning. This interesting phenomenon allows the rotor to sustain rotation at a certain rotational speed by balancing the aerodynamic torque acting on the blades. The insight into autorotation was first applied to air vehicles in the 1920s when the first autogyro was built and successfully flown by the pioneering engineer Juan de la Cierva (Ref. 1). Although autogyros were proved to provide significant advantages relative to other aircraft types, the greater operational envelope of the helicopter has relegated their use almost entirely to sport enthusiasts; hence they are less familiar to the wider public.

Autogyros have been built since the time of Cierva in a variety of design configurations. These range from amateur and sport enthusiasts' designs to fully certified aircraft. Several types of rotor systems have also been used. For example, the McDonnell Aircraft XV-1 convertiplane, which operated in an autogyro mode, had a unique hub design with a large delta-3 flap-coning arrangement to obtain positive stability characteristics (Refs. 2, 3). However, the most widely used rotor configuration is the semi-rigid teeter (see-saw) head system (Ref. 4). This hub configuration is simple and is found in most currently flown

autogyros, despite the fact that teetering rotors in low loading flight conditions (low G conditions) may suffer from reduced control authority, which can lead to mast bumping condition or excessive blade flapping (Refs. 4, 5). Furthermore, the lack of understanding of autogyro stability together with inadequately trained pilots resulted in a number of fatal accidents in the past. In the early 1990s, the UK Civil Aviation Authority (CAA) started to draw its attention to autogyro safety, particularly after a series of accidents between 1989 and 1991 (Ref. 6), which recorded an alarming average of 6 fatalities per 1000 hours of flying time. A safety review report published by the CAA in 2002 showed that although the number of fatal accidents has dropped in later years, the average fatalities per hours flown was astonishingly higher than any type of aircraft (Ref. 7).

In an attempt to categorize the autogyro crashes on the basis of their causes, the Popular Rotorcraft Association identified two major contributing issues related to the accident recorded (Ref. 8): Pilot Deficient Proficiency and Aircraft Instability (sometimes known as Aircraft Pitch Instability). Power failure, mechanical failure, object impact and wind can also be causes of autogyro accidents. The Aircraft Instability represents incidents where the aircraft becomes unstable and uncontrollable. There are many ways in which this instability can be manifested, including rapid pitch oscillations or maneuver, excessive vibrations, violent blade flapping leading to rotor blades striking on other aircraft components in-flight, loss of rotor speed and loss of control at high-speed flight or in turbulent wind. In the past few decades, there has been a number of studies, which investigated the aircraft stability of the full autogyro vehicle from a flight mechanics standpoint. Examples of these studies can be found in the work conducted by Houston *et al.* (Refs. 9–15), Sapthopoulos (Ref. 16), T. Thomson *et al.* (Refs. 6, 17, 18), Bagiev (Refs. 19, 20), Lopez and Wells (Ref. 21), Rigsby *et al.* (Refs. 22, 23), Hickey (Ref. 24) and CAA (Ref. 25).

For the rotor and blade related instabilities, there are also different ways in which they can manifest. For example: the inability of the rotor to sustain autorotation, unstable blade flapping or lead-lag motion, unstable blade bending or twist deformation as in blade flutter or divergence, etc. Furthermore, in certain conditions, the rotor can be considered stable yet it may exert excessive loads on the rotor hub. These loads may result in very large hub moments about the longitudinal and lateral hinges of the rotor head, which will be transmitted through the control system resulting in a strong control stick vibration condition, particularly for the rotor direct control case (Ref. 26). If the loads on the stick are higher than the pilot's

capacity, undesirable pilot-in-the-loop interactions can emerge, which in turn can result in the rotor tilting excessively about the longitudinal or lateral hinges. These situations can potentially lead to the blades making contact with other aircraft components. Therefore, autogyro rotor related instabilities can lead to inability to maintain autorotation, excessive blade motion or deformation or excessive rotor shaft tilt. These instabilities can, therefore, cause the blades to make contact with the other autogyro components, potentially resulting in dangerous or fatal accidents. Table 1 for instance, presents examples of three recorded accidents caused by rotor-related instabilities.

There has been a number of studies of the stability of autorotating blades in the past few decades. The following section gives a brief review of the studies found in the literature that are relevant to the topic. However, the main outcome from the review is that the autorotational stability of the rotor in forward flight is still not fully understood. Hence, this article tries to address this shortfall through experimentally and numerically assessing the blade autorotational stability of a scaled teetering rotor. The analysis is presented from the perspective of exploring the multi-attractor dynamics of the nonlinear rotor behavior. This approach is novel and was not used in previous studies that attempted to investigate the stability of autorotating rotors, apart from some of the authors' previous work which will be discussed below. In this article, the expression "autorotational stability" refers to the ability or inability of the rotor to maintain autorotation.

Following the review of autorotating rotor blade stability concepts and relevant studies, we present the bifurcation and continuation methods that form the basis of generating the numerical results and interpreting the experimental outputs. The research methodology is then described in detail followed by results and discussion.

Review on Rotor Blade Instability in Autorotation

As previously mentioned, autorotation is a phenomenon that relies on balancing the aerodynamic torque acting on the blades to create a stable state of rotation. One can question though if this autorotational state is always achievable. If it cannot be sustained during flight then a form of instability is developed. Insight concerning this scenario can simply be obtained by studying the aerodynamics around

a chosen blade element, as illustrated by Fig. 1. The forces acting on a section of the blade are dependent on the local inflow angle (ϕ) and the local angle of attack (α). In addition, the section aerofoil characteristics reflected in the lift and drag coefficients are also contributing factors to the magnitude of forces. If the blade section is at an autorotational equilibrium then the sum of the force components in the plane of rotation (horizontal axis) is zero. This results in the following equation:

$$D\cos\phi - L\sin\phi = 0 \tag{1}$$

Simplifying the equation in coefficient form by assuming small angles leads to:

$$C_d - C_l\phi = 0 \qquad or \qquad C_d/C_l = \phi = \alpha - \theta \tag{2}$$

C_l and C_d are the aerofoil lift and drag coefficients respectively. Equation (2) represents, for given values of θ, a series of parallel lines inclined by 45° when plotted in a C_d/C_l versus α diagram (Ref. 1), as shown in Fig. 2. This diagram is usually called an *autorotational diagram* and it was first used by Wimperis (Ref. 27). An equilibrium condition is denoted by point A, where the line intersects the measured C_d/C_l data. If the blade section operates in the concave region, say at point B, then the inflow angle will be greater than the measured C_d/C_l data. This means that the forward component of the lift is greater than the drag force components, which will result in an accelerating force. On the other hand, if the blade section operates in the convex region, say point C, a decelerating torque condition will be achieved.

From the stability point of view, the accelerating and decelerating forces at points B and C are actually stabilizing. For example, if the blade section is at point B, the inflow angle is high causing an accelerating forward force. This will increase the in-plane component of the flow velocity, which in turn will reduce the inflow angle. The equilibrium position will eventually be achieved. The autorotational diagram is constructed for a single (two dimensional) blade cross section. However, for the whole rotor blade, constructing a similar diagram may not be possible. This is because autorotation equilibrium, in this case, is determined by the cumulative effects of the forces and flow velocities acting along the whole blade.

The autorotation diagram depicted in Fig. 2 also shows that there is a maximum pitch angle θ_{max} above which autorotation is not possible, regardless of the inflow angle value. This state represents the blade element stall, which causes only a decelerating force condition to exist. For more information about the autorotation diagram, the reader is advised to consult Refs. 1, 28 and 29.

Nikolsky and Seckel (Ref. 30) extended the above analysis to rotors in axial autorotation. They considered the effect of stalling on the stability of autorotation. They showed that when stall effects are included, two trim solutions can be found. The first represents the normal stable autorotation state, while the other is an unstable autorotation condition. The analysis also revealed that for small blade incidences, the stability of the blade is evident. However, for higher blade incidences, there is a risk that flow disturbances can cause the blades to stall, because of the unstable trim points being close to the normal autorotation state. Nikolsky and Seckel also illustrated that there is a maximum of incidence(about 8.8° for the example rotor used) above which axial autorotation cannot exist.

However, they stated that the results obtained from this analysis should be considered purely as qualitative. This is because the induced velocity was assumed constant, which meant that the distribution of the angles of attack along the blade is not accurately predicted, and hence the stall contributions at high angles are also not properly accounted for. It was suggested that in order to have more confidence in this study, a better representation of the induced velocity and the drag at the stalled areas need to be used, as well as to account for the effect of Reynolds number on drag and lift across the blade.

The above analyses did not consider the effects of blade mechanical motion or elastic deformation. In fact, there is a significant shortage of studies investigating the behavior of a rigid autorotating rotor blade with flap and lead-lag degrees of freedom, compared with powered rotors. On the other hand, in 1936, Wheatley (Ref. 31) conducted an analysis to determine the main factors that govern the oscillations of the autogyro rotor blade in the plane of rotation. The findings illustrated that the lead-lag oscillations are mainly the direct effects of blade flapping through Coriolis forces and that the influence of the aerodynamic forces in the plane of rotation is secondary. The analysis was also endorsed by flight test validations.

In 1978, Wei and Peters (Ref. 32) studied the blade lag stability in autorotation. This was achieved by calculating the damping in the lag degree of freedom of rigid blades using perturbation methods, with spot checks using the Floquet method. The effects of advance ratio, blade elastic coupling, blade in-plane natural frequency and rotor trim condition were investigated. This analysis revealed that blades operating in the autorotation condition are considerably less stable compared to the powered flight regime,

particularly for soft in-plane rotors*. This study, was limited to cases of advance ratios less than 0.5. On the other hand, Rigsby (Ref. 23) used Floquet analysis to investigate the stability of an autorotating rotor but the analysis did not predict any form of blade instability, although the results identified some areas where the stability was reduced.

In a more recent study, Floros and Johnson (Refs. 33, 34) conducted an investigation into the blade flap-lag stability for compound helicopter configuration rotors using Floquet analysis. Different rotor hub configurations including articulated and teetering rotors were considered. The latter was that of the CarterCopter Technology Demonstrator (CCTD) (Ref. 35). The analysis used three rotor model types: an analytical rigid flapping blade, a rigid blade CAMRAD II model and an elastic blade CAMRAD II model (Ref. 36). Using the rigid blade CAMRAD II model for the CCTD rotor in the autogyro configuration, no instability was found up to an advance ratio of 2 and Lock number of 18. In fact, it was difficult to find trim solutions above those values. Furthermore, Floros and Johnson discussed the fact that the trim solution in autorotation is not unique, which raises the question of whether a maneuver could cause the rotor to change abruptly between different states. This issue was not considered in detail since it was beyond the scope of the analysis. Furthermore, although Floros and Johnson studied the blade stability in autorotation, the rotor speed was actually held constant during the process of computing the damping values. In other words, rotor speed degree of freedom was only considered to trim the rotor to autorotation state (zero net torque) and not for the stability analysis.

Another source of rotor instability in autogyros is the interaction between the blade elastic forces with the aerodynamic and inertial forces. Floros and Johnson (Ref. 33) used an elastic blade model in CAMRAD II to determine the effects of elasticity on blade stability. They showed that blade elasticity can drastically reduce the rotor stability. For the considered blade stiffnesses, it was predicted that a teetering rotor is unstable at an advance ratio of 1.5, independent of pitch frequency, although no significant effects on rotor performance were observed. In this investigation, the rotor speed degree of freedom was not taken into account in the calculation of the blade elastic modal damping.

Due to the uncontrolled rotor speed of the autorotating rotor, conducting a numerical analysis that takes into account the blade's modal characteristics can be more complex relative to the powered rotor

*S*oft in-plane* refers to rotor blades with their first lag frequency being less than the rotor speed.

condition. In the early 2000's, Somov *et al.* (Refs. 37–39) constructed a mathematical model, which incorporated dynamics of flexible blades. However, the work focused on using such a model for autogyro flight mechanics problems and not to assess the blade behavior. The results were used to carry out robust control studies of the Irkutsk A-002 gyroplane. As far as the stability of the blade is concerned, Trchalík *et al.* (Refs. 40, 41) investigated the aeroelastic stability boundaries of the autorotating rotor blades in axial and forward flight. The analysis revealed that there is a strong coupling between the rotor speed and the blade bending and torsional degrees of freedom. It was found that the rotor can be susceptible to a flutter instability that is different from conventional helicopter blade flutter. This instability can lead to an excessive drop of rotor speed. Although the analysis conducted by Trchalík *et al.* was entirely based on time history simulations, it was possible to construct a stability boundary plot involving the blade torsional stiffness and chordwise position of blade center of gravity.

Furthermore, CarterCopters (Ref. 42) stated that their experience confirms an instability problem (like a flutter or divergence) on the retreating rotor blade caused by the reverse flow shifting its aerodynamic center from $\frac{1}{4}$ chord to $\frac{3}{4}$ chord. This shifting of the aerodynamic center results in flapping instability of the blades as the advance ratio becomes higher. In addition, the problems of excessive blade bending or twisting have been known since the early days of the autogyro. Wheatley (Ref. 43) stated that excessive or unstable travel of the center of pressure and rotor vibration are troublesome problems, which are considerably affected by the periodic twist of the rotor blade. This twist occurs during blade flapping motion due to the interaction between the elastic, aerodynamic and inertial forces acting on the blade.

From an experimental perspective, there is extremely limited research in the available literature that addresses blade stability for autogyro rotors. One of the few attempts is that by De Silva (Ref. 44) who performed wind tunnel tests to quantify the extent of flapping at high advance ratios. The tests showed that as the advance ratio increases the amplitude of the blade flapping angles increases first linearly and then exponentially, depending on the rotor disc loading. However, the results of the experiments did not distinguish between real flapping instability and large flapping angles. Wheatley and Bioletti (Ref. 45) conducted wind tunnel tests of 10-foot diameter rotors. The tests offered valuable information regarding the effects of blade collective pitch, rotor solidity and cyclic pitch (feathering angle) on the rotor lift and drag characteristics in autorotation. Although the objective of the tests was to collect performance data,

experimental findings showed that there is a critical angle of attack (rotor tilt) below which the rotor can self-autorotate and above which the rotor would rotate in the reverse direction. This critical angle was found to be about 20° for a collective pitch of 0° and about 8° for a pitch angle of 6°. It should be noted however, that the blades did not have a flap or a teetering degree of freedom, since the lift on the advancing and retreating sides of the rotor disc was balanced by a form of cyclic pitch mechanism. Therefore, since the rotor has only one degree of freedom, manifested in the azimuthal rotation, it can spin either in normal autorotation or in a reverse direction. Here, normal autorotation refers to the rotor spinning condition where the flow passes from the blade leading edge to the trailing edge.

As far as rotor characteristics at high advance ratios are concerned, one of the early wind tunnel investigations was conducted by Jenkins (Ref. 46). He studied the performance characteristics of a 15-foot diameter teeter rotor at advance ratios between 0.65 and 1.45. One of the interesting results was the discovery of a *thrust reversal* phenomenon. Unlike the case where the advance ratio is less than 1, an increase in collective pitch angle now leads to a reduction in rotor thrust for a constant disc attitude, for advance ratios higher than 1. Jenkins argued that this reversal phenomenon might be troublesome for pilots with manual control. Although the tests were conducted at a fixed rotor speed, thrust reversal can also occur for autorotating rotors. The investigation did not, however, mention any sign of flap instability.

In summary, it can be seen from this brief literature review that the research carried out so far on autorotating blade stability is still not conclusive. In particular, the effects of stall on the autorotational stability, the existence of more than one autorotation state and the interaction between the blade flap dynamics and the rotational degree of freedom require further investigation. In an attempt to address some of these research gaps, which suggest nonlinearity in the system, the authors have conducted a number of studies in recent years, using numerical continuation and bifurcation methods, and wind-tunnel testing. For example, in (Ref. 47), the coexistence of stable and unstable branches in the behavior of autogyro rotors was demonstrated, both numerically and experimentally. The implications of such nonlinear behavior on the stability of autogyros from an engineering and flight safety perspective were discussed in (Ref. 48). In subsequent work (Ref. 49), the benefits of the combined numerical-experimental approach in studying the dynamics of nonlinear fluid-structure problems, as in the case of an autorotating rotor, were highlighted.

In this article, the partially understood problem of autogyro blade flap-rotation instability in forward flight is revisited. The results of extended experimental tests complemented by numerical analysis are presented to reveal that the rotor instability is governed by the nonlinear characteristics of the autorotating rotor; specifically, it will be shown how the loss of rotor stability is related to dependencies on the blade stall at advance ratios close to 1.

Continuation and Bifurcation Methods for Rotorcraft Problems

In the aerospace sector, the use of nonlinear methods such as continuation and bifurcation tools is becoming more widespread. In particular, these methods are increasingly adopted to investigate nonlinear aircraft flight dynamics and control problems. However, the application of continuation and bifurcation methods has been limited to a small number of helicopter dynamical problems, such as flight mechanics (Refs. 50–56), ground resonance (Refs. 57, 58) and examination of the rotor vortex ring state (Ref. 59). Furthermore, almost all of the investigations which utilize these nonlinear tools can be regarded as research studies and it is still hard to find these tools widely adopted in industry for production aircraft. In recent years, the nonlinear aeroelastic stability of helicopter rotor blades was investigated by Rezgui *et al.* (Refs. 60, 61), using numerical continuation and bifurcation techniques. This investigation showed that these techniques are powerful in the identification of instability scenarios of rotor blades and uncovering the multiple solution structure driven by the nonlinearities in the rotor system. Moreover, this work led to the first practical application of the continuation and bifurcation methods for certification of production aircraft, which contributed towards the latest Release-To-Service of the AW159/Wildcat helicopter (Ref. 62).

The basic idea of numerical continuation and bifurcation techniques is the calculation of the steady solutions of a dynamical system as one of its parameters, called the continuation parameter, is varied across a pre-defined range. The computed solutions construct a set of branches that could be either stable or unstable. The continuation is the branch-following algorithm that generates these solutions. To determine their stability, either an eigen or Floquet analysis is carried out at each computed solution, depending on the nature of the solution. For instance, in axial autorotation, the blade behavior can be considered to be

in equilibrium (*fixed points*), hence an eigen analysis is carried out for stability, whereas in forward flight and due to the rotor lift asymmetry condition, the blades behave in a periodic manner constituting what is known as *limit cycle oscillations*. Therefore, Floquet theory is used to determine the stability of these limit cycles.

A bifurcation is a qualitative change in the system behavior as a parameter is varied. In other words, when the stability of a system is changed or lost, the system bifurcates. The points at which these stability changes happen are called bifurcation points. When the system is nonlinear, new solution branches may emerge from the bifurcation points, leading to the presence of multiple solutions for the same set of system parameters. The identification of these different solution branches helps to uncover the global dynamics of the system. The different types of bifurcations that can occur in equilibria or periodic orbits are not discussed in this paper; the reader is referred to general texts such as reference (Ref. 63) for more background on the subject.

Therefore, the strategy in implementing continuation and bifurcation methods is to follow one solution branch as one or more parameters are varied to locate bifurcation points. The emerging branches are then followed to construct a more complete picture of the system dynamics, producing what is known as a bifurcation diagram. The advantages of continuation methods, compared with other time history or frequency domain methods, are their efficiency and accuracy in following the solution branches and in detecting as well as identifying the bifurcation points. The numerical tools used for bifurcation analysis can vary from simple brute-force time-integration techniques to the so-called numerical continuation methods. However, the accuracy and the correctness of the results produced by these tools are greatly dependent on the fidelity and validity of the nonlinear dynamical models used.

There are several freely available continuation software with different levels of maturity and robustness. AUTO (Ref. 64), Continuation Core (COCO) (Ref. 65), MATCONT (Ref. 66) and CL_MATCONT (Ref. 66) are examples of the most widely used packages. In this analysis, the continuation and bifurcation software AUTO was used. AUTO is open source software for continuation and bifurcation problems of ordinary differential equations (as well as other types of problems), originally developed by Eusebius Doedel, with subsequent major contributions by several researchers; it is currently available on a number of platforms (Refs. 64, 67). Besides many other types of equations, AUTO can perform extensive

bifurcation analysis of ordinary differential equations of the form:

$$\dot{x}(t) = f(x(t), p), \quad x \in \Re^n, p \in \Re^m, f : \Re^n \times \Re^m \longrightarrow \Re^n \tag{3}$$

subject to initial conditions, boundary conditions, and integral constraints. Here x is the state vector and p denotes one or more parameters. n and m are the numbers of states and parameters respectively. Equation (3) is written in the generic nonlinear state-space form, where the state-derivatives are functions of the states and some parameters. The continuation algorithms implemented in AUTO allows the direct calculations of steady solutions (equilibrium or periodic solutions) as the continuation parameters are varied from previously computed solutions, without the need to conduct time history simulations. The continuation algorithms use numerical iteration and collocation schemes as appropriate to compute stable as well as unstable solutions more efficiently than many other numerical schemes.

The main type of steady solution which describes the rotor blade behavior in the conventional forward flight operating envelope is the periodic orbit (limit cycle). Unlike a helicopter, an autogyro rotor in forward flight autorotation has a variable rotational speed. Hence the rotor is not forced to rotate at a fixed frequency and the blade azimuthal angle would then need to be modeled as a state variable. The rotor in forward autorotation is, therefore, a self-excited dynamical system.

Methodology and Analysis

The first objective of the analysis is to trace the steady state solutions when the rotor is in autorotation over a range of parameters. The wind speed, the shaft angle and the blade pitch angle are the three parameters of interest in this investigation. Initially, the investigation was done experimentally through a series of wind tunnel tests using a scaled autogyro model specifically designed for this study. The effect of changing the initial value of rotor speed was also studied to get an insight into the stability of the rotor. Next, a numerical analysis was conducted using continuation and bifurcation methods. The dynamics of the scaled autogyro rotor operating in autorotation was modeled in Matlab as a low order nonlinear dynamical model. The steady periodic solutions and their stability were then determined using the continuation and bifurcation software AUTO.

Description of Experiment

The experiments were performed in the University of Bristol low speed open jet wind tunnel. The wind tunnel is a closed return system with a 1.68m long open working section. The diameter of the jet is 1.1m and the maximum attainable velocity is about 33m/s. The experimental rig (see Fig. 3(a)) comprises a two bladed teeter rotor of 1m in diameter. The blades are rigidly connected and free to flap about a hinge located at the shaft axis. The blades have a rectangular planform with no twist and are connected to the rotor hub at a radial position of 0.1 m. The blade chord, mass, Lock number and aerofoil section are 62 mm, 0.15 kg, 47.1 and NACA0015 respectively. The skeleton of the rotor rig, including the hub system, is modified from a radio controlled helicopter. The flapping angle of the blades (teetering angle) is measured using a magnetic encoder which has a resolution of $0.15^\circ \pm 0.07^\circ$. The pitch of each blade can be pre-set at the hub without the need of a swashplate and the blade pitch angle is monitored using separate magnetic encoders that are connected to each blade via a pulley and tooth belt system, resulting in a total pitch resolution of $0.15^\circ \pm 0.07^\circ$. The signals from these three sensors are transmitted via a ZigBee-based wireless telemetry to a Personal Computer.

The rotor speed and azimuthal position are monitored using an optical encoder connected to the rotor shaft. This encoder is connected to the PC via a dSPACE interface. A six-component load cell (JR3-100M40A) fitted below the fuselage is used to measure the forces and moments acting on the rotor rig. The airframe is designed to closely represent a scaled version of the Magni VPM-16 autogyro, modified by having a closed cockpit. The purpose of this airframe is to cover the components of the rotor support frame and provide a smoother aerodynamic shape, and hence was not designed to match the scale of the rotor dimensions. Finally, a safety mechanism is implemented to prevent damage to the rotor rig should the blade motions become unstable (see Fig. 3(b)). This mechanism is located in the rotor hub and uses two spring-loaded valves which are released by a mechanical locking system when contacted by a blade exceeding the maximum allowed flapping angle of 23°.

The procedure was to measure the rotor speed and blade flapping angles in autorotation, as the wind speed (U), shaft angle (θ_{shaft}) or blade collective pitch angle (θ_{col}) were varied. The first series of tests were conducted at a collective pitch angle of 1°. In each test, the shaft angle was inclined at a chosen

value, where the blade flapping angle and rotational speed were recorded as the rotor was subjected to different wind speeds, taken at 1 m/s intervals. The aerodynamic forces and moments were also measured. At every wind speed value, the rotor was allowed enough time to settle down to steady autorotation, then the readings for the flapping angle and rotational speed were recorded for 30 seconds, whereas the aerodynamic forces were recorded for 6 seconds. These experiments were repeated twice to ensure reproducibility of the results. The rotor often required to be pre-rotated (by hand or using string wound around the shaft) for the first test point to allow autorotation to take place. This set of experiments was repeated for collective pitch angles of -1°, 0°, 2° and 3°.

It is worth noting that some measurements were not possible due to unforeseen rotor shaft vibration (shaft resonance), which often occurred when the rotor rotated close to average speeds of 500 rpm ($\pm 1\%$), 960 rpm ($\pm 1\%$) and 1270 rpm ($\pm 1\%$). The last two frequencies were the most potentially damaging ones for the rotor and hence it was not practical to keep the rotor spinning close to those speeds if excessive vibration occurred. Operating the rig close to those resonance conditions also affected the accuracy of the measurement to the extent that large discrepancies in rotor speed and flap angle were observed. Excluding those cases, the maximum scatter in the measured rotor speed was about 35 rpm and in the flapping angle amplitudes about 1.5 deg.

The next step of the experiment was to identify, within the wind speed range, any areas where the blade dynamics change. This was done in two stages. Firstly, by investigating the rotor behavior at the high and low limits of achievable wind speeds. Secondly, by perturbing the rotor velocity during the normal autorotation regimes. This was simply achieved by introducing a level of friction force for a short period of time, enough to slow the rotor down to a target rotor speed.

Description of Numerical Rotor Model

It was anticipated that the rotor dynamics could display some nonlinear behavior. Therefore, in order to properly investigate the stability of rotor dynamics numerically, it was necessary to use nonlinear analysis methods with an adequate numerical model. In this investigation, a low order nonlinear rotor model that retained acceptable fidelity in the aerodynamic and dynamic representations was created. Since the focus

was the rotor stability associated with the blade rigid degrees of freedom, it was adequate to assume rigid blades free to rotate at the root in and out of the plane of rotation. The model describes the dynamics of a two-bladed teetering rotor. It was formulated in the nonlinear state-space form as: $\dot{x} = f(x, p)$, where $x \in \mathbb{R}^n$ is the state vector, $p \in \mathbb{R}^m$ is a vector of m parameters (e.g. blade pitch angle, wind speed, etc.) and f is the set of n nonlinear equations (equations of motion and inflow model). The following simplifying assumptions – demonstrated to provide reasonable model performance output for autorotating rotors (Ref. 68) – are adopted in the aerodynamic representation:

The model was based on a two-dimensional steady aerodynamics blade element approach, where lift and drag forces at each element are calculated numerically using nonlinear look-up tables as functions of angle of attack and Reynolds number. Experimental data for a NACA0015 aerofoil section is used for each blade element (Ref. 69). Since it is of interest to investigate high advance ratio conditions, in which reverse flow is expected to occur over a portion of the rotor disc, the look-up tables cover the whole 360° range of angle of attack. To obtain the elemental lift and drag forces, the flow velocity components, inflow angle and angle of attack are first calculated at each element, see illustration in Fig. 1. Then, the elemental thrust, torque and aerodynamic moment about the flap (teetering) hinge are computed from the lift and drag values. Integrating the elemental airload contributions from the root to the tip of the blade gives the total thrust, torque and flapping moment for each blade. The compressibility effects were neglected because the blade tip speed is generally low in autorotation even at high forward speed, due to low rotor speed. For simplicity, blade/blade and blade/hub interactions were ignored. Furthermore, tip losses were approximated by assuming that the lift forces at the tip reduce to zero. For this analysis, a tip loss factor of 97% was used.

Instead of describing flapping by its Fourier components in the non-rotating frame, the individual flapping coordinate, β, is retained for each blade and also its azimuthal position, ψ. For the teetering rotor, both blades are assumed to be rigidly connected and hence have one flapping degree of freedom; also, blade rotation together with blade lead-lag motion are represented by the same state variable, namely the rotational degree of freedom around the shaft axis, ψ. There is no pre-defined coning to the rotor blades and hence the blade flapping angle is equivalent to the rotor teetering angle. The blades' coordinates were therefore allocated by choosing a default blade as shown in Table 2. The flapping coordinate for the

blades, β, is dependent on ψ. The differential equations of the rotor in both the flapping and the rotation senses are second order, giving a total of four rotor states (ψ, $\dot{\psi}$, β and $\dot{\beta}$).

The equations of motion were formulated to include the effects of an autogyro flight dynamics on the rotor blades' behavior. Transformation of velocity, acceleration and force components were used in a vector form between different coordinate systems. The full derivations of equations are beyond the scope of this paper and can be found in Ref. 70. However, for completeness a compact form of the equations used for the teetering rotor are reproduced here:

$$\ddot{\psi} = (N_{\psi,1} + N_{\psi,2})/(2I_{blade}\cos\beta) \tag{4}$$

$$\ddot{\beta} = (M_{\beta,1} - M_{\beta,2})/(2I_{blade}) \tag{5}$$

where

$$N_{\psi,i} = (N_{aero,i} - M_{blade}(a^{shaft}_{hub,i})_y) - [(P^{shaft}_i \cos\beta_i - R^{shaft}_i \sin\beta_i) \times (Q^{shaft}_i + \dot{\beta}_i) - (\alpha^{shaft}_{hub,i})_x \sin\beta_i - (\alpha^{disc}_{hub})_z \cos\beta_i] I_{blade}$$

$$M_{\beta,i} = (M_{aero,i} + M_{blade}((a^{shaft}_{hub,i})_x \sin\beta_i + (a^{shaft}_{hub,i})_z \cos\beta_i)) + \left[(P^{shaft}_i \cos\beta_i - R^{shaft}_i \sin\beta_i) \times (P^{shaft}_i \sin\beta_i + R^{shaft}_i \cos\beta_i) - (\alpha^{shaft}_{hub,i})_y\right] I_{blade}$$

where $N_{\psi,i}$ and $M_{\beta,i}$ are the overall torque and flapping moment respectively on blade i and $N_{aero,i}$ and $M_{aero,i}$ are the aerodynamic torque and flapping moment, respectively for each blade i. M_{blade} and I_{blade} are the blade mass moment and second moment of inertia respectively. P^{shaft}_i, Q^{shaft}_i and R^{shaft}_i are the angular velocities of the rotor hub in the shaft axes. $a^{shaft}_{hub,i}$ and $\alpha^{shaft}_{hub,i}$ are the translational and angular acceleration vectors of the hub in the shaft axes respectively. α^{disc}_{hub} is the angular acceleration vector of the hub in the rotor disc axes. The main coordinate systems used in Eqs. 4 and 5 are illustrated in Fig. 4. Furthermore, the inertial loads were calculated by evaluating the acceleration vectors acting at any radial position on the blade, in the blade coordinate system. These vectors included the dynamic contributions of the aircraft and hub movements as well as the rotational, flapping and lead-lag motion of the blades. Therefore, the inertial forces acting on any blade element were obtained, which allowed by the process of

integration to calculate the inertial forces and moments acting on both blades.

The induced flow through the rotor is captured via a three-state dynamic wake model, originally developed by Pitt and Peters (Refs. 71–74) for helicopter rotors. The version of inflow model used here was that by Houston *et al* (Ref. 14, 75, 76), which was adapted for rotors operating in autorotation. The three-state inflow model is given as:

$$\nu_i(r,\psi) = \nu_0 + \frac{r}{R}(\nu_s \sin\psi + \nu_c \cos\psi) \tag{6}$$

where ν_i is the induced velocity at the i^{th} element of radius r and R is the blade tip radius. The induced velocity components ν_0, ν_s and ν_c are given in the wind axes by:

$$[\tau]\begin{bmatrix}\dot{\nu}_0\\ \dot{\nu}_s\\ \dot{\nu}_c\end{bmatrix}_{wind} = -\begin{bmatrix}\nu_0\\ \nu_s\\ \nu_c\end{bmatrix}_{wind} + [L]\begin{bmatrix}T_{aero}\\ L_{aero}\\ M_{aero}\end{bmatrix}_{wind} \tag{7}$$

where

$$[\tau] = \begin{bmatrix} \frac{4R}{3\pi\nu_T} & 0 & \frac{-R\tan(\chi/2)}{12\nu_m} \\ 0 & \frac{64R}{45\pi\nu_m(1+\cos\chi)} & 0 \\ \frac{5R\tan(\chi/2)}{8\nu_T} & 0 & \frac{64R}{45\pi\nu_m(1+\cos\chi)} \end{bmatrix} \tag{8}$$

and

$$[L] = \frac{1}{\rho\pi R^3}\begin{bmatrix} \frac{R}{2\nu_T} & 0 & \frac{15\pi\tan(\chi/2)}{64\nu_m} \\ 0 & \frac{-4}{\nu_m(1+\cos\chi)} & 0 \\ \frac{15\pi R\tan(\chi/2)}{64\nu_T} & 0 & \frac{-4\cos\chi}{\nu_m(1+\cos\chi)} \end{bmatrix} \tag{9}$$

T_{aero}, L_{aero} and M_{aero} are the thrust, the aerodynamic lateral and pitching moments respectively in the wind axes and the skew angle χ can be obtained from:

$$\chi = \text{atan}\left(\frac{\sqrt{u_{hub}^2 + v_{hub}^2}}{\nu_{i,m} - w_{hub}}\right) \tag{10}$$

where the 'quadrant-arctangent' function (`atan2` function in Matlab) is used in Eq. (10) to compute the correct value of the wake skew angle. ν_T and ν_m are expressed as:

$$\nu_T = \sqrt{u_{hub}^2 + v_{hub}^2 + (\nu_{i,m} - w_{hub})^2} \tag{11}$$

$$\nu_m = \frac{u_{hub}^2 + v_{hub}^2 + (\nu_{i,m} - w_{hub})(2\nu_{i,m} - w_{hub})}{\nu_T} \tag{12}$$

where u_{hub}, v_{hub} and w_{hub} are the flow velocity components relative to the rotor hub, and $\nu_{i,m}$ is the induced velocity from momentum theory, which can be evaluated using the Glauert equation (Ref. 77).

The model was implemented in MATLAB and has seven states, where the state vector is

$$x = [\psi,\ \dot{\psi},\ \beta,\ \dot{\beta},\ \nu_0,\ \nu_s,\ \nu_c]^T.$$

A number of the model parameters can be used as continuation parameters. However, to understand the rotor stability during operational conditions, the main parameters of concern are flow speed (U), preset collective pitch angle of the blades (θ_{col}) and rotor shaft tilt angle relative to the flow (θ_{shaft}); the latter is subsequently referred to as simply 'shaft angle'.

The blade dimensions, mass and aerofoil aerodynamic characteristics of the experimental autogyro blade were used in the numerical model. Initial spot checks using time history simulations predicted rotor speed values much greater than those achieved in the wind tunnel tests. The main reason for this large difference in rotor speed was believed to be the simple aerodynamic representation used in the model. This discrepancy in rotor speed also led to dissimilarities in other aspects of the model, notably the rotor flapping angle and forces produced by the rotor. Further scrutiny of the results revealed that the high value of the predicted autorotational speed is related to the poor estimation of the rotor aerodynamic torque, which caused the torque balance to be realized at higher rotor speeds than those measured experimentally.

Therefore, a simple model-tuning task was conducted to correct for some of the aerodynamic characteristics that were not accounted for or were not accurately modeled, such as airframe and tunnel interaction effects, inaccurate rotor downwash, etc. For simplicity, it was decided to use a friction term in the rotation sense of the rotor, representing an added resisting aerodynamic torque, to correct for those misrepresented characteristics. The use of this crude assumption was not expected to produce an exact match between the numerical and the physical model for all the rotor states. However, the rationale was that this correction would narrow the discrepancy gap and produce a reasonable match in rotor speed, at the same operating parameters, without increasing the complexity of the model. Furthermore, in reality, an amount of resisting torque was present in the rotor shaft due to friction in the hub bearings and the swash plate.

The frictional torque correction term is assumed proportional to the rotational blade velocity:

$$T_{Friction} = \zeta \cdot \Omega \tag{13}$$

where $\zeta = f_1(\theta_{shaft}) + f_2(\theta_{col})$ is a friction ratio and is a function of both the shaft and the blade collective pitch angles. The following functions for f_1 and f_2 were found to provide a reasonable fit to the experimental data:

$$f_1(\theta_{shaft}) = 10^{-3} \cdot (-0.225\theta_{shaft}^2 + 2.99\theta_{shaft} - 2.94) \tag{14}$$

$$f_2(\theta_{col}) = 10^{-3} \cdot (0.45\theta_{col}^{0.7}) \tag{15}$$

where the shaft and blade pitch angles in the above equations are in degrees. The tuning of the friction coefficient ζ was based on trimming the rotor model by only matching the rotor speeds to those found in the experiment at the stable autorotation branches. It should be noted that it was not possible to trim the numerical model at low values of forward speed (below 25m/s for shaft angle of 7° and pitch of 1deg). However, this was resolved by extrapolating the experimental rotor speed values above the 30m/s limit of the wind tunnel. The nonlinear least square curve method in Matlab (`lsqnonlin`) was used to fit the torque coefficient data gathered to the function described in Eqs (14) and (15). Finally, it should be noted that even if the rotor speed is well tuned, the other states are not expected to be closely matched because of this crude experimental correction. However, it was expected that an adequate rotor speed match would allow the model to produce at least a qualitative agreement with the experiment.

Results and Discussion

Nonlinear Stability of the Autorotating Rotor

Figures 5 and 6 depicts the variation of the measured rotational speed and flapping angle at steady autorotation state, for two blade pitch settings: $\theta_{col} = 1^\circ$ and $\theta_{col} = 0^\circ$ respectively. Since the recorded flapping data was periodic with rotor azimuth position, the average peak values for each cycle were computed over the period of the data recording. These peak values of the oscillating flapping angle were plotted for different tunnel speed values and rotor shaft angles. For the rotor velocity, the averaged mean values were used instead since the variation in rotor speed due to the blade lead-lag motion was very

small, see Fig. 7. The steady periodic behavior of the rotor presented in Figs 5 and 6 demonstrated that the rotor not only achieved stable autorotation but also maintained this stable periodic condition despite the flow perturbations inherent in the wind tunnel. The best-fit curves for the measured data were also plotted. These curves were extrapolated to obtain an illustration of the rotor speed and peak flapping angle variations at higher wind speeds. The results illustrate that the rotational velocity increased almost linearly with the forward wind speed, while the flapping angle had an inverse relationship with the wind speed.

The experiment also revealed that at each setting of shaft angle, autorotation was not possible below a certain wind speed value, which indicated the presence of an instability point - in other words, the presence of a bifurcation point. Instead, regardless of how high (within the permissible range) or low the initial value of the rotor speed was, the blades' rotational speed always decayed and the flapping oscillation diverged until the blades made contact with the safety mechanism, which was activated at about 23 degrees of flapping angle. It should be noted that it was difficult to precisely determine the minimum airspeed at which stable autorotation was possible, particularly with the adverse effects of tunnel flow perturbations. Therefore, the instability points illustrated in Figs. 5 and 6 were located within a ± 1.5 m/s band of the indicated wind speed value.

The subsequent experiment was to test the ability of the rotor to achieve stable autorotation state at flow speeds higher than the minimum autorotation airspeed, but in this case starting from different low initial rotor speeds. To achieve a level of control in the initial rotor speed values, the rotor was first operated in stable autorotation at a chosen wind tunnel speed. Next, a level of frictional torque was manually applied at the rotor shaft to reduce the rotor speed down to a desired value. The top of the wireless telemetry shroud was found to be the best place to apply this resisting torque. Figure 8 depicts the results for different initial rotor speeds when the shaft angle was set to 7°. After repeating the tests a few times, it was possible to define a rotor speed boundary (presented by a red dashed line in Fig. 8), which separated qualitatively different rotor behaviors. At this boundary, the rotor appears to be in steady autorotation but due to the presence of flow disturbances it transitioned away to the stable autorotation state on one side. On the other side of the boundary, the blade flapping oscillations grew excessively, leading to the safety mechanism being activated. This rotor speed boundary represented an unstable periodic branch of

rotor dynamics in autorotation, which was characterized by lower rotor speed and larger flapping angle magnitudes, compared with the stable autorotation state.

The diagrams in Fig. 8 resemble experimental bifurcation diagrams of the physical teetering rotor. They show the presence of stable and unstable autorotation branches, which connect at the bifurcation point. Because of the latter and also because of the unidirectional transient behavior of the blades at wind speeds below the bifurcation point, the instability point resembles a *fold bifurcation*: it defines the minimum wind speed value for which steady autorotation will exist. Moreover, the approach used to find the above bifurcation diagrams is typically known as a *brute-force bifurcation* method, which was implemented in an experimental setting in this case.

To further investigate the above results, different continuation runs were performed for the tuned numerical model, representing the physical rotor rig. The results are shown in Fig. 9, which presents the bifurcation diagrams with the wind speed as the continuation parameter for various rotor shaft angles and for a blade collective pitch of 1°. The bifurcation diagrams clearly illustrate the existence not only of the stable and unstable period autorotation branches but also of fold bifurcation points. However, the fold points are located at higher wind speeds compared to those recorded during wind tunnel tests. Fig. 9 also shows that the shape of the stable autorotation branches (rotor velocity and flapping angle) are very similar to those obtained from experiments (see Fig. 5). Moreover, the profile of unstable branches near the bifurcation points was also well predicted, confirming the relatively sharp structure of the steady state rotor speed solutions close to bifurcation points. These results confirmed that the nonlinear stability of a rotor in autorotation can be predicted - at least qualitatively- using continuation and bifurcation techniques, despite the relative simplicity of the numerical model and updating process. The continuation analysis also detected fold bifurcation points, which can be difficult to predict by other methods. Indeed, some approaches may mistakenly suggest unstable solutions in the region where there should be none, such as beyond a fold point where there is no local solution branch.

Figure 9 also illustrates that as the shaft angle is reduced the fold bifurcation points occurs not only at higher wind speeds but also when the rotor is spinning at higher rotor speeds. A similar result can also be observed experimentally from Fig. 5, despite the fact that increase in rotor speed of the fold point was only about 300 rpm between the cases of $\theta_{shaft} = 10^\circ$ and 4°.

Effects of Rotor Loading and Advance Ratio in Autorotation

The location of the bifurcation point found during the experiments as the shaft angle was changed was investigated next. Figure 10 illustrates a two-parameter experimental bifurcation diagram and shows that the wind speed value at which the fold bifurcation occurs increases as the shaft angle is reduced. This implies that the fold bifurcation points also specify the minimum permissible shaft angle required for autorotation at a given wind speed value. In order to clarify the effects of the above results on autogyro flight performance, the average aerodynamic lift values generated by the rotor are superimposed as contours in the same figure. Figure 10 (a) indicates that the fold bifurcation line lies in an area where the rotor produces low values of lift (below 1 N to just above 3 N compared with a maximum measured lift of approximately 30 N). This shows that when the rotor is unloaded by reducing the shaft angle or the flow wind speed, its stability will be determined by whether or not the fold bifurcation line is crossed. Furthermore, the higher the wind speed the higher the minimum lift value generated by the rotor. This means that the minimum permissible lift value increases at higher wind speed. This is an important result because, for autogyros flying at high-speed level flight, the rotor shaft angle needs to be reduced to maintain the lift and weight balance. If the shaft angle is reduced enough so that the fold bifurcation point is reached then the rotor will no longer be able to sustain stable autorotation. Instead, the rotor speed will decay and the blades will flap in an oscillatory divergent manner.

In Fig. 10 (b), the variation of the measured advance ratios for stable autorotation is plotted versus wind speed and shaft angle. Superimposing the fold bifurcation line in the same figure reveals that the fold bifurcation occurs at an advance ratio close to 1. In fact, even when the blade pitch angle was set to $\theta_{col} = 0^\circ$ or $\theta_{col} = 2^\circ$ the fold bifurcation occurred at advance ratios close to 1, see Fig. 11. This finding endorses the proposition that autorotating rotors are susceptible to instability at high advance ratios.

In an attempt to understand the factors associated with the rotor instability the distribution of blade angles of attack and torque were investigated using the tuned numerical model. Figure 12 depicts the variation of the elemental blade angles of attack at stable autorotation, for a shaft angle setting of $\theta_{shaft} = 7^\circ$, a blade pitch of $\theta_{col} = 1^\circ$ and at two different wind speeds. The first speed represents a point very close to the fold bifurcation point (27 m/s), while the second is chosen to be far from the bifurcation (40 m/s)

for comparison. The figure shows that close to the fold, the retreating blade is essentially operating in a stalled condition. In addition, the angles of attack at the inboard blade section of the advancing side are quite high (over 10°). This means that the magnitude of the accelerating torque is small, which can be seen from Fig. 13 where the torque values are small (and not diverse) compared to the case of $U = 40$ m/s.

These results meant that the fold bifurcation is associated with the blade stall condition, which causes the inability of the rotor to sustain autorotation. These results are therefore the general case of the studies by Wimperis (Ref. 27) and Nikolsky and Seckel (Ref. 30) discussed in the second section of this article. However, those studies only considered the effect of high collective pitch angle on simple autorotation cases (blade element or simple blade in axial autorotation). Therefore, the work presented here extends the previous findings and confirms, both experimentally and numerically, that there are at least two steady states of autorotation in the forward flight case for autorotating rotors (one stable and one unstable).

Effect of Blade Pitch

Finally, the effects of changing the blades' collective pitch angle were investigated. The shaft angle chosen for this case was $\theta_{shaft} = 7°$. Attempts to get the rotor to autorotate at θ_{col} lower than $-2°$ and θ_{col} higher than 4° did not succeed over the available speed range of the tunnel. Figure 14 depicts the variation of rotor lift and advance ratio versus blade pitch angle and wind speed. It can be seen that the fold bifurcation line still lies in an area where the rotor produces low values of lift and where the advance ratio is close to 1. Figure 15 shows the variation of the measured rotor speed and blade flapping angle corresponding to Fig. 14. This illustrates that the stability boundary defined by the fold bifurcation line occurs at lower rotor speeds and higher flapping angles compared with the normal stable autorotating conditions.

Furthermore, it can be seen that in the range of 11 m/s and 17.5 m/s, two bifurcation points exist at every wind speed: one at a small collective pitch angle and another at a higher angle. For example, at $U = 16$ m/s, two fold bifurcation points exist at approximately $\theta_{col} = -0.9°$ and 2.5°. From this plot, one can easily visualize the appropriate bifurcation diagram for the case of $U = 16$ m/s, when the pitch angle is taken as the continuation parameter. Figure 16 depicts this experimental bifurcation diagram. For

$\theta_{col} = 0^\circ$ and 2°, the mean rotor speeds and the peak flapping angles at the unstable branch were found in a similar way to that used in Fig. 8. Figure 16 clearly illustrates that autorotation is only possible within a range of blade pitch angles, which is dependent on wind speed and shaft angle. At the limits of this range, there are two fold bifurcations that define the points at which the torque balance in the rotor cease to exist. This type of bifurcation diagram is usually called an *isola*, since the stable and unstable branches form a closed solution branch that is isolated from any other dynamics (if other solutions exist). The above results represent a new qualitative interpretation of autorotating rotor stability.

The dual periodic behavior (stable and unstable solutions) displayed by the rotor in autorotation can suggest that other solutions (attractors or repellers) might exist, this could provide insight to a more global view of the system behavior. In fact, one instance of the rotor in stable operation at wind speeds below that of the fold bifurcation points was observed. It seemed during the experiments that all attempts to operate the rotor in these low wind speed cases ended up by activating the safety mechanism, due to the large flapping oscillations before the rotor speed decayed to a halt. This one contrary observation indicated that at low wind speeds the rotor might be attracted to a different stable periodic attractor, residing beyond the limits of the maximum flapping angle. The analysis of this finding falls beyond the objectives of this article and is detailed in the authors' work in Ref. 48 and Ref. 49.

Finally, to determine if the tuned numerical model can also provide similar behavior to that of wind tunnel test when the blade collective pitch angle is varied, continuation runs were performed for $\theta_{shaft} = 7^\circ$ and wind speeds of 30 m/s, 34 m/s and 40 m/s. The results as shown in Fig. 17 depict that the numerical bifurcation diagrams are qualitatively similar to those obtained during the experiments (shown in Fig. 16) and clearly confirm that autorotation is possible only within a range of blade pitch angle. At the limits of this range (minima and maxima of operational collective pitch angles), fold bifurcations exist and they define the points beyond which autorotation is impossible. These bifurcation diagrams also confirm that the stable and unstable branches for each wind speed case constitute an *isola*.

It can be seen in Fig. 17 that the collective pitch angle range for autorotation to exist reduces as wind speed is decreased. At the flow speed of 40 m/s the maximum allowed blade pitch angle for stable autorotation is about 4°, whereas it is slightly less than 2° at 30 m/s. This result indicates that having the ability to reduce the blade pitch angle during flight can allow stable autorotation at slower forward speeds

or higher advance ratios. In general, both experimental and numerical results confirmed the dependence of fold bifurcations on the collective pitch. Therefore, blade twist and torsional flexibility, as well as blade aerofoil sectional properties, can also be important parameters that can influence the blade stability for a full-size autogyro rotor. For example, blades with significant flexibility in twist can lead to scenarios where the effective blade pitch angle is outside the fold points, leading to unstable behavior.

Conclusions

A stability analysis of a scaled autogyro teetering rotor using wind tunnel tests and numerical continuation was presented. The analysis focused on the rotation-flap stability of the autorotating blades. The experimental analysis was carried out using a 1 m diameter rotor with two rigid blades connected at a flapping (teetering) hinge, which is located at the rotor shaft. The tests investigated the steady periodic behavior of the autorotating rotor for a range of parameters, namely wind tunnel speed, rotor shaft tilt angle relative to the airflow and blade collective pitch angle. For the numerical analysis, an experimentally-tuned low order nonlinear rotor model based on a blade element approach was developed. The continuation and bifurcation analysis software AUTO was then used to compute the steady periodic solutions and assess their stability using Floquet analysis. The main conclusions of the work presented in this paper are:

- The rotor instability in autorotation is associated with the existence of fold bifurcations, which define regions within the parameter space where autorotation is not possible. These bifurcations occur predominantly at lightly loaded conditions (when the rotor is producing low values of lift) and at advance ratios close to 1, for the scaled autogyro model. The fold bifurcations define the conditions at which the torque balance in the rotor ceases to exist. Furthermore, it was revealed that the inability of the rotor to autorotate is associated with blade stall.
- The continuation analysis detected fold bifurcation points, which can be difficult to predict by other methods. Indeed, some approaches may mistakenly suggest unstable solutions in the region where there should be none, such as beyond a fold point where there is no local solution branch.
- Both stable and unstable autorotation states (periodic behavior) exist for the teetering rotor. The unstable autorotation state was shown to act as a threshold, which roughly indicates the minimum

initial rotor speed condition for a stable autorotation to take place. In other words, the analysis can be used to predict the target minimum rotor speed required in the manual or motorized pre-rotation phase of the full-scale autogyro rotor, which is usually required before take off. Moreover, the unstable rotor speed branches can be used to set minimum rotor speed limits during steady flight or maneuvers, particularly those associated with low G conditions as in the push-over maneuver.

- Autorotation is only possible within a small range of blade pitch angles, which is dependent on wind speed and shaft angle. The stable and unstable autorotative periodic behavior of the rotor forms what is known as an *isola*, where two fold bifurcations exist at the minimum and maximum allowed collective pitch angle. These two points define the limits of the range of conditions at which the torque balance in the rotor can exist. These results represent a new qualitative interpretation of autorotating rotor stability in forward flight.

- Lastly, the numerical results were qualitatively in good agreement with those generated from the wind tunnel experiments. As demonstrated for the rotor system, the combined numerical-experimental procedure facilitated a new insight into the nonlinear nature of the autorotating blade behavior, which provided a better explanation of autogyro rotor instability. The methods can be used to establish stability boundaries in the design and operational parameter space.

Finally, the study of nonlinear stability of autorotating rotors and autogyros is still in its infancy. For future work, therefore, the continuation and bifurcation analysis can be used to predict the nonlinear stability of a full-size rotor/autogyro, particularly to investigate low G, rotor speed decay and thrust-reversal conditions. In addition, work to enhance the numerical model is needed to obtain a better quantitative agreement with experiment; a particular focus will be to enhance the prediction of aerodynamic torque and to develop a simple inflow model better suited to low rotor speed conditions. Another recommendation is to investigate how the bifurcation diagram can manifest for different rotor hub arrangements and assess how design parameters can affect the stability boundaries within the flight envelope.

Acknowledgment

The authors would like to thank the Algerian Ministry for Higher Education and Scientific Research for funding the work presented in this paper. The authors are also very grateful to Mr Peter C. Bunniss from the University of Bristol for his continuous support and guidance throughout the undertaking of the work.

References

[1]Leishman J. G. "Development of the Autogyro: A Technical Perspective," *Journal of Aircraft*, Vol. 41, (4), July–August 2004, pp. 765–781.

[2]Hohenemser K. "A Type of Lifting Rotor with Inherent Stability," *Journal of the Aeronautical Sciences*, Vol. 17, (9), 1950, pp. 555–564.

[3]Harris F. "An Overview of Autogyros and the McDonnell XV1 Convertiplane," Nasa Contractor Report-2003-212799, NASA, October 2003.

[4]Transportation U.S. Department of and Administration Federal Aviation. *Rotorcraft Flying Handbook*, CreateSpace Independent Publishing Platform, 2013.

[5]Leishman J. G. *Principles of Helicopter Aerodynamics*, Cambridge University Press, 2000.

[6]Thomson D. G. and Houston S. S. "Advances in Understanding Autogyro Flight Dynamics," American Helicopter Society 64^{th} Annual Forum Proceedings, Montreal, Canada, April 29–May 1, 2008.

[7]Authority Civil Aviation. "Aviation Safety Review 1992–2001," Technical Report CAP 735, Safety Regulation Group, Civil Aviation Authority, October 2002.

[8]Popular Rotorcraft Association PRA. "Safety Report: Gyroplane Accident Causes per NTSB Report," 2002.

[9]Houston S. S. "Validation of Non-linear Individual Blade Rotorcraft Flight Dynamics Model Using Perturbation Method," *Aeronautical Journal*, Vol. 98, (977), August–September 1994, pp. 260–266.

[10]Houston S. S. "Longitudinal Stability of Gyroplanes," *Aeronautical Journal*, Vol. 100, (991), 1996, pp. 1–6.

[11]Houston S. S. "Identification of Autogyro Longitudinal Stability and Control Characteristics," *Journal of Guidance, Control and Dynamics*, Vol. 21, (3), May–June 1998, pp. 391–398.

[12]Houston S. S. "Identification of Gyroplane Lateral/Directional Stability and Control Characteristics from Flight Test," Proceedings of the Institution of Mechanical Engineers, Part G: Journal of Aerospace Engineering, Vol. 212, (4), 1998, pp. 271–285.

[13]Houston S. S. "Validation of Rotorcraft Mathematical Model for Autogyro Simulation," *Journal of Aircraft*, Vol. 37, (3), May–June 2000, pp. 403–409.

[14]Houston S. S. and Brown R. E. "Rotor Wake Modelling for Simulation of Helicopter Flight Mechanics in Autorotation," *Journal of Aircraft*, Vol. 40, (5), September–October 2003, pp. 938–945.

[15]Houston S. S. "Modelling and Analysis of Helicopter Flight Mechanics in Autorotation," *Journal of Aircraft*, Vol. 40, (4), July–August 2003, pp. 675–682.

[16]Spathopoulos V. M. "Validation of a Rotorcraft Mathematical Model in Autorotation by Use of Gyroplane Flight Tests," *The Aeronautical Journal*, Vol. 108, (1079), 2004, pp. 51–58.

[17]Thomson D. G., Houston S. S., and Spathopoulos. "Experiments in Autogyro Airworthiness for Improved Handling Qualities," *Journal of the American Helicopter Society*, Vol. 50, (4), October 2005, pp. 295–301.

[18]Thomson D. G. and Houston S. S. "Application of Parameter Estimation to Improved Autogyro Simulation Model Fidelity," *Journal of Aircraft*, Vol. 42, (1), January–February 2005, pp. 33–40.

[19]Bagiev M., Thomson D. G., and Houston S. S. "Autogyro Inverse Simulation for Handling Qualities Assessment," Proceedings of 29th European Rotorcraft Forum, Friedrichshafen, Germany, September 16–18, 2003.

[20]Bagiev M. and Thomson D. G. "Handling Qualities Evaluation of an Autogiro against the Existing Rotorcraft Criteria," *Journal of Aircraft*, Vol. 46, (1), January–February 2009, pp. 168–174.

[21]Lopez C. A. and Wells V. L. "Dynamics and Stability of an Autorotating Rotor/Wing Unmanned Aircraft," *Journal of Guidance, Control and Dynamics*, Vol. 21, (3), May–June 1998, pp. 391–398.

[22]Rigsby J. M. 'Stability and Control Issues Associated with Lightly Loaded Rotors Autorotating in High Advancing Ratio Flight," American Helicopter Society 64^{th} Annual Forum Proceedings, Montreal, Canada, April 29–May 1, 2008.

[23]Rigsby J. M. *Stability and Control Issues Associated with Lightly Loaded Rotors Autorotating in High Advancing Ratio Flight*, PhD thesis, Georgia Institute of Technology, December 1990.

[24]Hickey D. H. "Full-Scale Wind Tunnel Tests of the Longitudinal Stability and Control Characteristics of the XV-1 Convertiplane in the Autorotating Flight Range," NACA Technical Report, RM. A55K21a, NASA, May 1965.

[25](CAA) Civil Aviation Authority. "The Aerodynamics of Gyroplanes," Technical Report CAA Paper 2009/02, UK Safety Regulation Group, CAA, 2009.

[26]Bailey F. J. "Flight Investigation of Control-Stick Vibration of the YG-1B Autogyro," NACA Technical Report, TN. No. 764, NASA, June 1940.

[27]Wimperies H. E. "The Rotating Wing in Aircraft," Technical Report R & M No. 1108, Aeronautical Research Council, 1926.

[28]Nikolsky A.A. *Notes on Helicopter Design Theory: A Series of Lectures Delivered March-April 1944 at Princeton University*, Princeton University Press, 1944.

[29]Gessow A. and Myers G. C. *Aerodynamics of the Helicopter*, Macmillan New York, 1952, republished by Frederick Ungar Publishing, New York, 1967.

[30]Nikolsky A. A. and Seckel E. "An Analytical Study of the Steady Vertical Descent in Autorotation of Single Rotor Helicopters," NACA Technical report, TN. No. 1906, NASA, 1949.

[31]Wheatley J. B. "A Study of Autogiro Rotor-Blade Oscillations in the Plane of the Rotor Disc," NACA Technical Report, TN. No. 581, NASA, September 1936.

[32]Wei F-S. and Peters D.A. "Lag Damping in Autorotation by a Perturbation Method," American Helicopter Society 34^{th} Annual Forum Proceedings, Washington, D.C., May 15–17, 1978, pp. 78–25.

[33]Floros M. W. and Johnson W. "Stability Analysis of the Slowed–Rotor Compound Helicopter Configuration," American Helicopter Society 60^{th} Annual Forum Proceedings, Baltimore. MD., June 7–10, 2004.

[34]Floros M. W. and Johnson W. "Stability and Control Analysis of the Slowed–Rotor Compound Helicopter Configuration," *Journal of the American Helicopter Society*, Vol. 52, (3), July 2007.

[35]Carter Jr J. "Cartercopter - a High Technology Gyroplane," American Helicopter Society Vertical Lift Aircraft Design Conference Proceedings, San Fransisco, CA, January 2000.

[36]Johnson W. "Rotorcraft Aeromechanics Applications of a Comprehensive Analysis," American Helicopter Society Vertical Lift Aircraft Design Conference Proceedings, Nagarafukumitsu, Gifu, Japan, April 1998.

[37]Somov Ye. I. and Polyntsev O. Ye. "Nonlinear Dynamics and Control of a Wind–Milling Gyroplane Rotor," International Conference on Physics and Control, 1(PHYCON'03), August 2003, pp. 151–156.

[38]Somov Ye. I. and Polyntsev O. Ye. "Nonlinear Dynamics of Gyroplane Rotor," Preprint of the 16th IFAC Symposium on Automatic Control in Aerospace, 1, 2004, pp. 565–570.

[39]Somov Ye. I. and Polyntsev O. Ye. "Nonlinear Dynamics and Robust Control of Gyroplane Rotor," The 16th IFAC (International Federation of Automatic Control) World Congress, 2005, pp. 3–8.

[40]Trchalík J., Gillies E. A., and Thomson D. G. "Aeroelastic Behaviour of a Gyroplane Rotor in Axial Descent and Forward Flight," Proceedings of 32nd European Rotorcraft Forum, Maastricht, The Netherlands, September 12-14, 2006.

[41]Trchalík J., Gillies E. A., and Thomson D. G. "Development of an Aeroelastic Stability Boundary for a Rotor in Autorotation," American Helicopter Society Specialist Conference on Aeromechanics, January 2008.

[42]Carter, J., "Extreme Mu Rotor," US Patent 6,986,642, 2006.

[43]Wheatley J. B. "An Analysis of the Factors that Determine the Periodic Twist of an Autogyro Rotor Blade, with Comparison of Predicted and Measured Results," NACA Technical Report No. 600, 1937.

[44]De Silva S. *Investigation of Autogyro Rotor Flapping Instability at High Forward Speed,* MEng Thesis, Bristol University, May 2000.

[45]Wheatley J. B. and Bioletti C. "Wind–Tunnel Tests of a 10-foot Diameter Gyroplane Rotor," NACA Technical Report No. 536, 1936.

[46]Jenkins J. L. "Wind–Tunnel Investigation of a Lifting Rotor Operating at Tip–Speed Ratios from 0.65 to 1.45," NASA Technical Report TN D-2628, February 1965.

[47]Rezgui D., Lowenberg M. H., and Bunniss P. C. "A Combined Numerical/Experimental Continuation Approach Applied to Nonlinear Rotor Dynamics," In *Progress in Industrial Mathematics at ECMI 2008*, Springer Berlin Heidelberg, Mathematics in Industry, London, UK, 2010, pp. 169–174.

[48]Rezgui D., Lowenberg M. H., and Bunniss P. C. "Experimental and Numerical Analysis of the Stability of an Autogyro Teetering Rotor," American Helicopter Society 64^{th} Annual Forum Proceedings, Montreal, Canada, April 29–May 1, 2008.

[49]Rezgui D. and Lowenberg M. H. "On the Nonlinear Dynamics of a Rotor in Autorotation: a Combined Experimental and Numerical approach," *Philosophical Transactions of the Royal Society of London A: Mathematical, Physical and Engineering Sciences*, Vol. 373, (2051), 2015.

[50]Sibilski K. "Bifurcation Analysis of a Helicopter Non–Linear Dynamics," *Archive of Mechanical Engineering*, Vol. 46, (2), 1999, pp. 171–192.

[51]Sibilski K. "Non–Linear Flight Mechanics of a Helicopter Analysis by Application of a Continuation Methods," Proceedings of the 25^{th} European Rotorcraft Forum, H4, Rome, Italy, September 14–16, 1999.

[52]Sibilski K. "A Study of the Flight Dynamics of Helicopter Carrying an External Load Using Bifurcation Theory and Continuation Methods," *Journal Of Theoretical and Applied Mechanics*, Vol. 41, (4), 2003, pp. 823 – 852.

[53]Bedford R. G. and Lowenberg M. H. "Use of Bifurcation Analysis in the Design and Analysis of Helicopter Flight Control Systems," Proceedings of the 29^{th} European Rotorcraft Forum, Friedrichshafen, Germany, September 16–18, 2003.

[54]Bedford R. G. and Lowenberg M. H. "Bifurcation Analysis of Rotorcraft Dynamics with an Underslung Load," Proceedings of the AIAA Atmospheric Flight Mechanics Conference, Providence, Rhode Island, August 16–19, 2004, pp. 595–619.

[55]Bedford R. G. and Lowenberg M. H. "Flight Dynamics Analysis of Periodically Forced Rotorcraft Model," Proceedings of the AIAA Atmospheric Flight Mechanics Conference, Keystone, Colorado, August 21–24, 2006, pp. 1210–1228.

[56]Maradakis G.S. *Fundamental Nonlinear Characteristics of Helicopter Flight Mechanics,* Master's Thesis, Dept. of Applied Mathematics, Glasgow Caledonian University, Glasgow, UK, December 2000.

[57]Mokrane A. *Helicopter Ground Resonance Prediction Using an Integrated Nonlinear Model*, PhD Thesis, Department of Aerospace Engineering, University of Bristol, Bristol, UK, 2011.

[58]Avanzini G. and De Matteis G. "Effects of Nonlinearities on Ground Resonance Instability," Proceedings of the 34^{th} European Rotorcraft Forum, Liverpool, UK, September 14-16, 2008.

[59]Basset P. M. and Prasad J. V. R. "Study of the Vortex Ring State Using Bifurcation Theory," American Helicopter Society 58^{th} Annual Forum Proceedings, Montreal, Canada, June 11–13, 2002.

[60]Rezgui D., Lowenberg M. H., Jones M., and Monteggia C. "Application of Continuation and Bifurcation Methods to Aeroelastic Rotor Blade Stability," Proceedings of 37^{th} European Rotorcraft Forum, Milan, Italy, September 13-15, 2011.

[61]D. Rezgui, M. H. Lowenberg, M. Jones, and C. Monteggia. "Continuation and Bifurcation Analysis in Helicopter Aeroelastic Stability Problems," *AIAA Journal of Guidance, Control, and Dynamics*, Vol. 37, (3), 2014, pp. 889–897.

[62]Jones M., Bernascone A., Masarati P., Quaranta G., and Rezgui D. "Ongoing Developments in the Use of Continuation–Bifurcation Methodology at AgustaWestland," Proceedings of 40^{th} European Rotorcraft Forum, Southampton, UK, September 2-5 , 2014.

[63]Kuznetsov Y.A. *Elements of Applied Bifurcation Theory*. Springer-Verlag, 1995, chap. 3–5.

[64]Doedel E. J., Oldeman B. E., Champneys A. R., Dercole F., Fairgrieve T. F., Kuznetsov Y. A., Paffenroth R. C., Sandstede B., Wang X. J., and Zhang C. "AUTO-07P : Continuation and Bifurcation Software for Ordinary Differential Equations," Technical Report, Concordia University, Montreal, Canada, 2009.

[65]Dankowicz H. and Schilder F. *Recipes for Continuation*, Science and Engineering. Society for Industrial and Applied Mathematics (SIAM), Philadelphia, PA, 2013.

[66]Dhooge A., Govaerts W., and Kuznetsov Y. A. "Matcont: a MATLAB Package for Numerical Bifurcation Analysis of ODEs," *ACM Transactions on Mathematical Software (TOMS)*, Vol. 29, (2), 2003, pp. 141–164.

[67]Coetzee E., Krauskopf B., and Lowenberg M. "The Dynamical System Toolbox: Integrating AUTO into MATLAB," The 16^{th} US National Congress of Theoretical and Applied Mechanics, USNCTAM2010–827, University Park, PA., June 27–July 2, 2010.

[68]Wheatley J. B. "An Aerodynamic Analysis of the Autogiro Rotor with a Comparison between Calculated and Experimental Results," NACA Technical Report 487, National Advisory Committee for Aeronautics, Langley Aeronautical Lab, United States, January 1934.

[69]Sheldahl R. E. and Klimas P. C. "Aerodynamic Characteristics of Seven Airfoil Sections Through

180 Degrees Angle of Attack for Use in Aerodynamic Analysis of Vertical Axis Wind Turbines," SAND80-2114, Sandia National Laboratories, Albuquerque, New Mexico, March 1981.

[70]Rezgui D. *Investigation into Rotor Blade Stability in Autorotation Using Bifurcation and Continuation Methods*, PhD Thesis, Department of Aerospace Engineering, University of Bristol, Bristol, UK, 2009.

[71]Pitt D.M. and Peters D.A. "Theoretical Prediction of Dynamic Inflow Derivatives," *Vertica*, Vol. 5, (1), 1981, pp. 21–34.

[72]Peters D. A. and HaQuang N. "Dynamic Inflow for Practical Applications," *Journal of American Helicopter Society*, Vol. 33, (4), 1988, pp. 64–68.

[73]Gaonkar G.H. and Peters D.A. "Review of Dynamic Inflow Modelling for Rotorcraft Flight Dynamics," *Vertica*, Vol. 12, (3), 1988, pp. 213–242.

[74]Chen R.T.N. "A Survey of Nonuniform Inflow Models for Rotorcraft Flight Dynamics and Control Applications," *Vertica*, Vol. 14, (2), 1990, pp. 147–184.

[75]Houston S.S. "Analysis of Rotorcraft Flight Dynamics in Autorotation," *Journal of Guidance, Control and Dynamics*, Vol. 27, (2), March–April 2004, pp. 258–269.

[76]Brown R.E. and Houston S.S. "Comparison of Induced Helicopter Velocity Models for Helicopter Flight Mechanics," *Journal of Aircraft*, Vol. 37, (4), July–August 2000, pp. 623–629.

[77]Glauert H. "A General Theory of the Autogyro," Aeronautical Research Council R&M 1111, 1926.

[78]Authority Civil Aviation. "Aviation Safety Review 1990–1999," Technical report CAP 701, Safety Regulation Group, Civil Aviation Authority, October 2000.

[79]Authority Civil Aviation. "Aviation Safety Review 2005," Technical report CAP 763, Safety Regulation Group, Civil Aviation Authority, August 2006.

[80]Authority Civil Aviation. "Aviation Safety Review 2008," Technical report CAP 780, Safety Regulation Group, Civil Aviation Authority, November 2002.

List of Figures

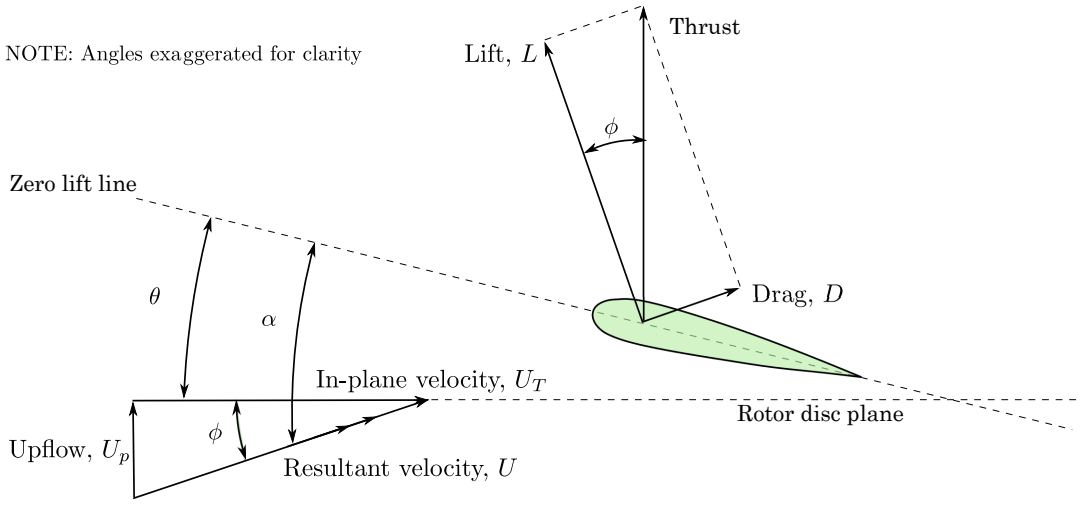

Fig. 1 Schematic diagram illustrating the flow and force components for a blade element in autorotation.

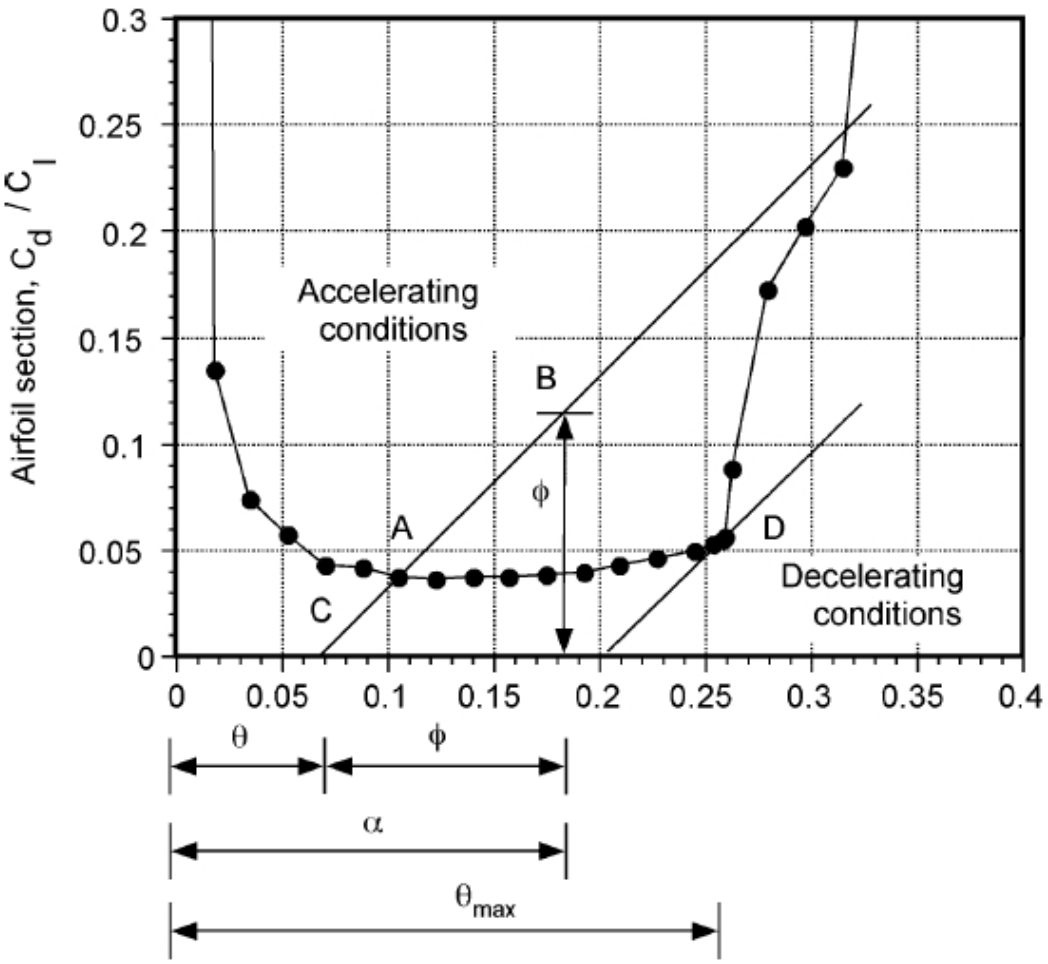

Fig. 2 Autorotational diagram in the form first suggested by Wimperis. From Ref. 1.

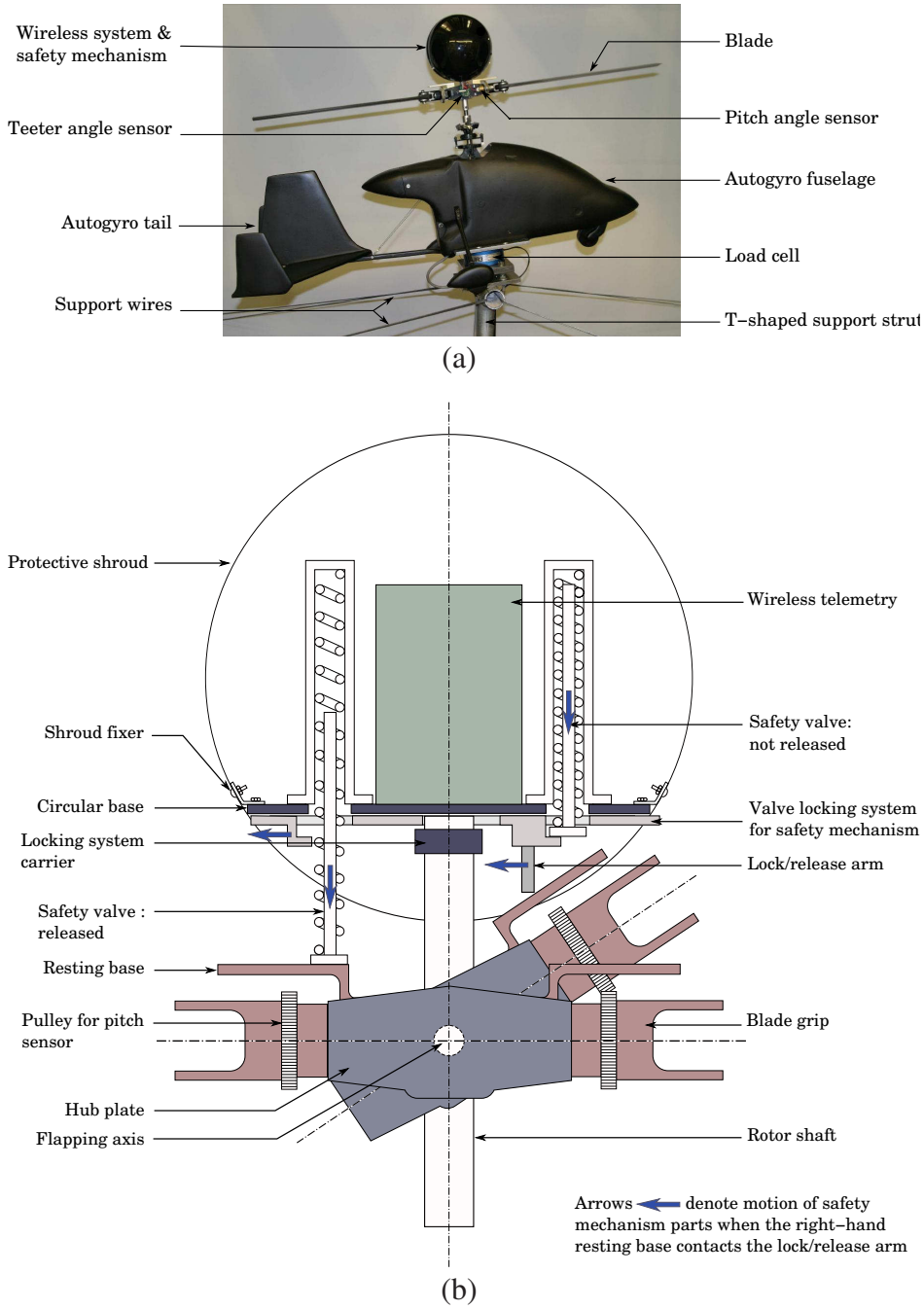

Fig. 3 Schematic view of the autogyro experimental rig used in wind tunnel. (a) The autogyro rig; the sphere above the rotor houses the wireless telemetry and safety mechanism. (b) Schematic view of the rotor hub, the wireless telemetry and safety mechanism.

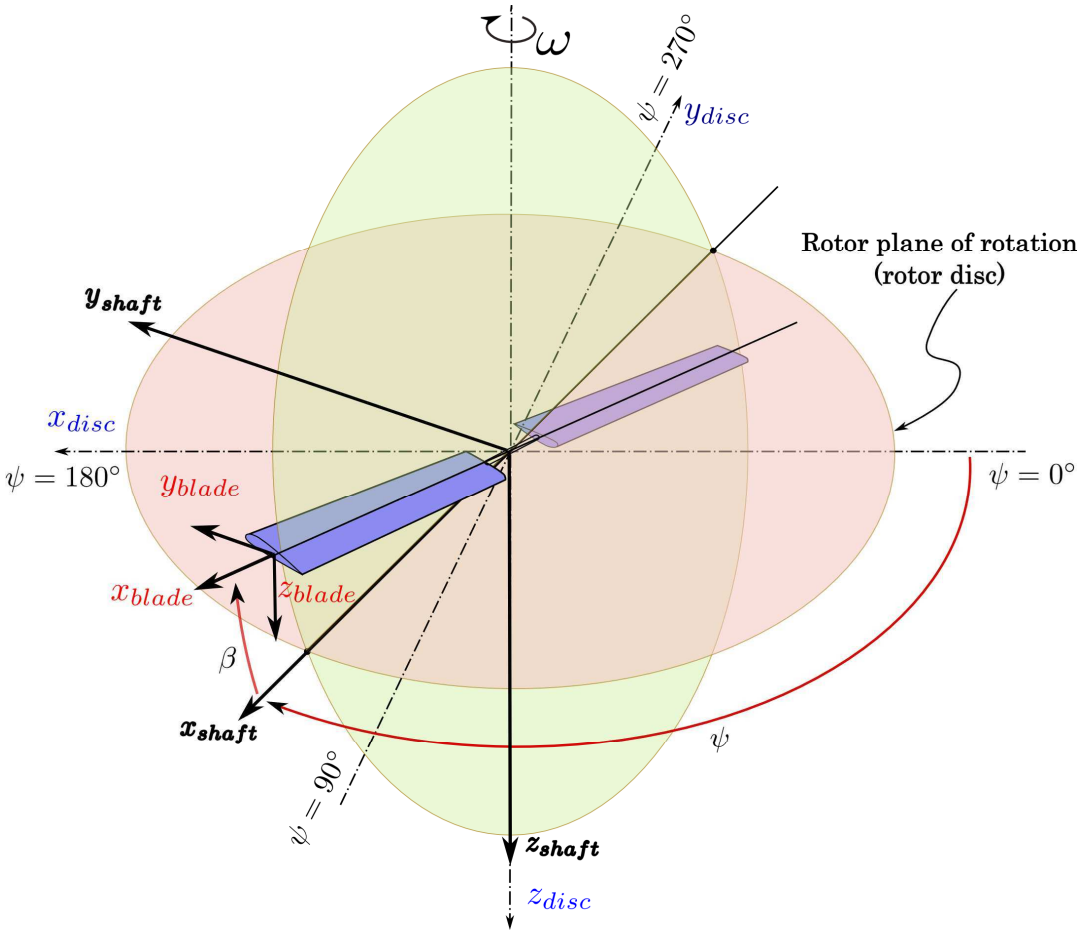

Fig. 4 Schematic diagram illustrating transformation from disc to shaft and blade coordinate systems.

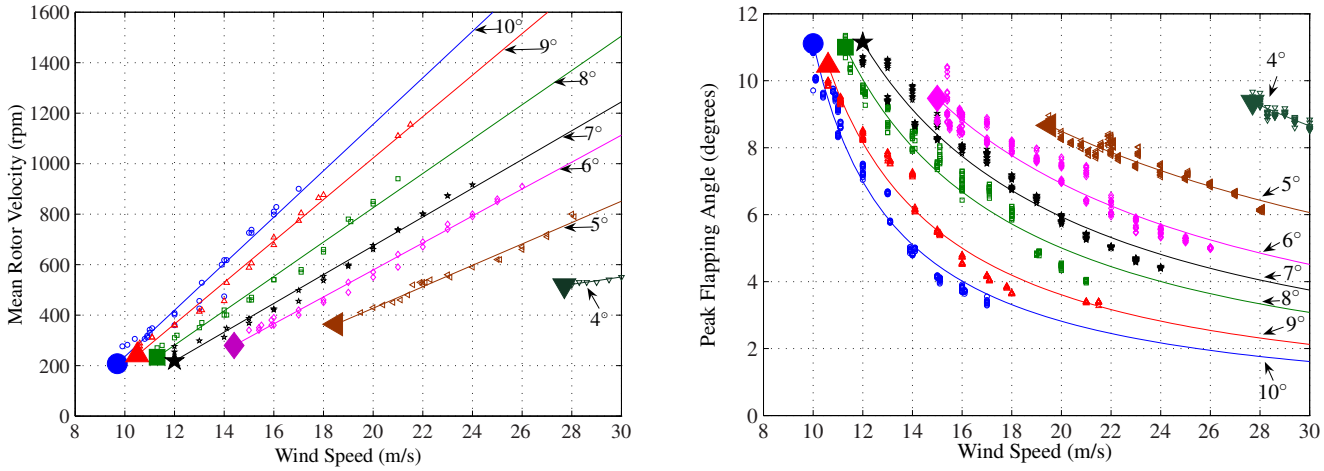

Fig. 5 Variation of (a) rotor velocity and (b) blade flapping angle max. amplitudes with tunnel wind speed and rotor shaft angle (labeled) for $\theta_{col} = 1°$. The large solid markers define the wind speed value below which the rotor can not sustain steady autorotation.

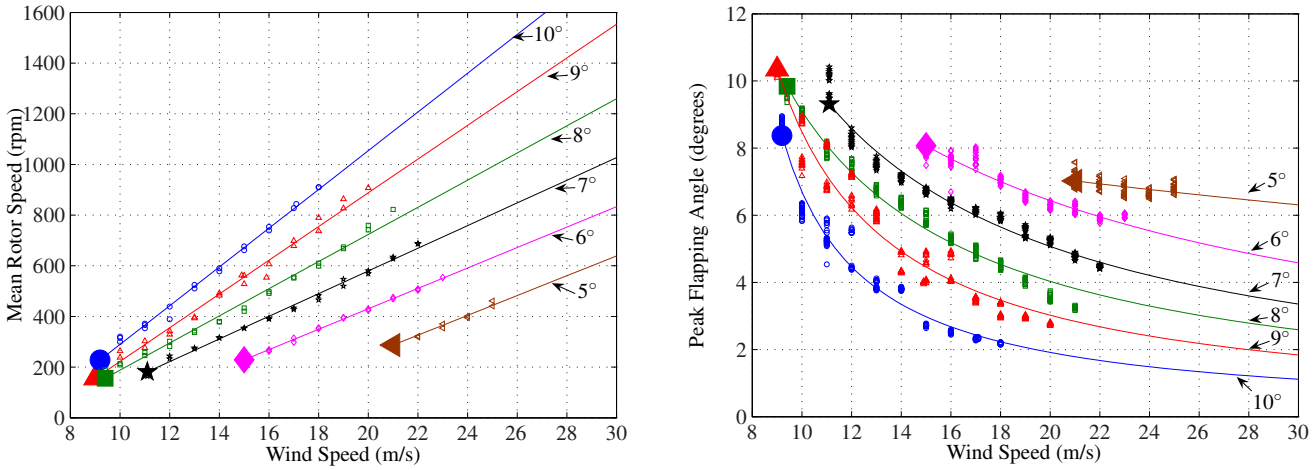

Fig. 6 Variation of (a) rotor velocity (from Ref. 49) and (b) blade flapping angle max. amplitudes with tunnel wind speed and rotor shaft angle (labeled) for $\theta_{col} = 0°$. The large solid markers define the wind speed value below which the rotor can not sustain steady autorotation.

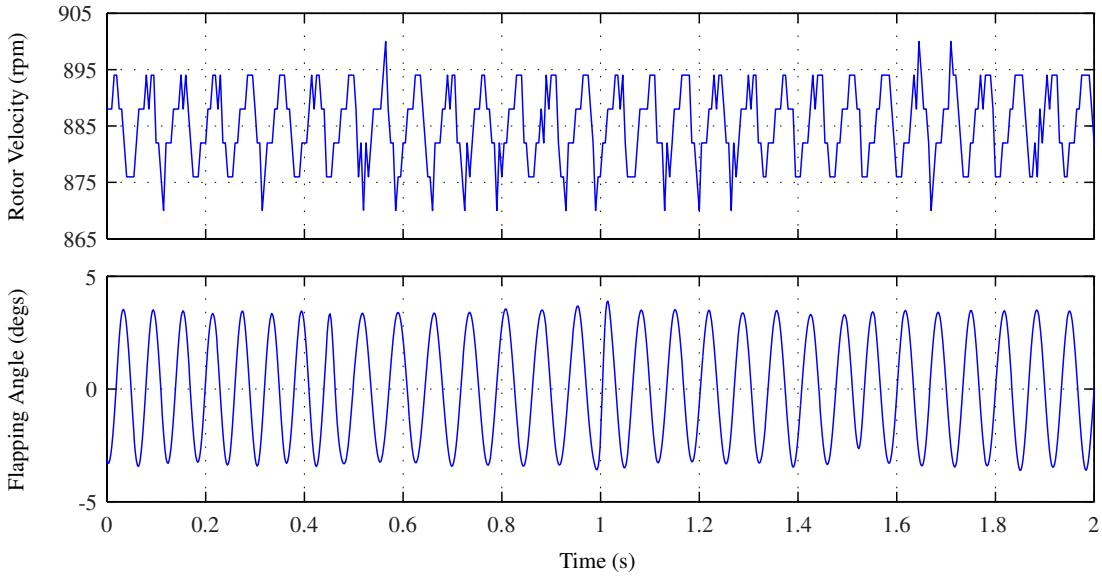

Fig. 7 Measured rotor velocity and flapping angle for $\theta_{col} = 1^\circ$ at $\theta_{shaft} = 10^\circ$ and $U = 17$ m/s. Note: the rotor velocity and flapping angle readings are not synchronized.

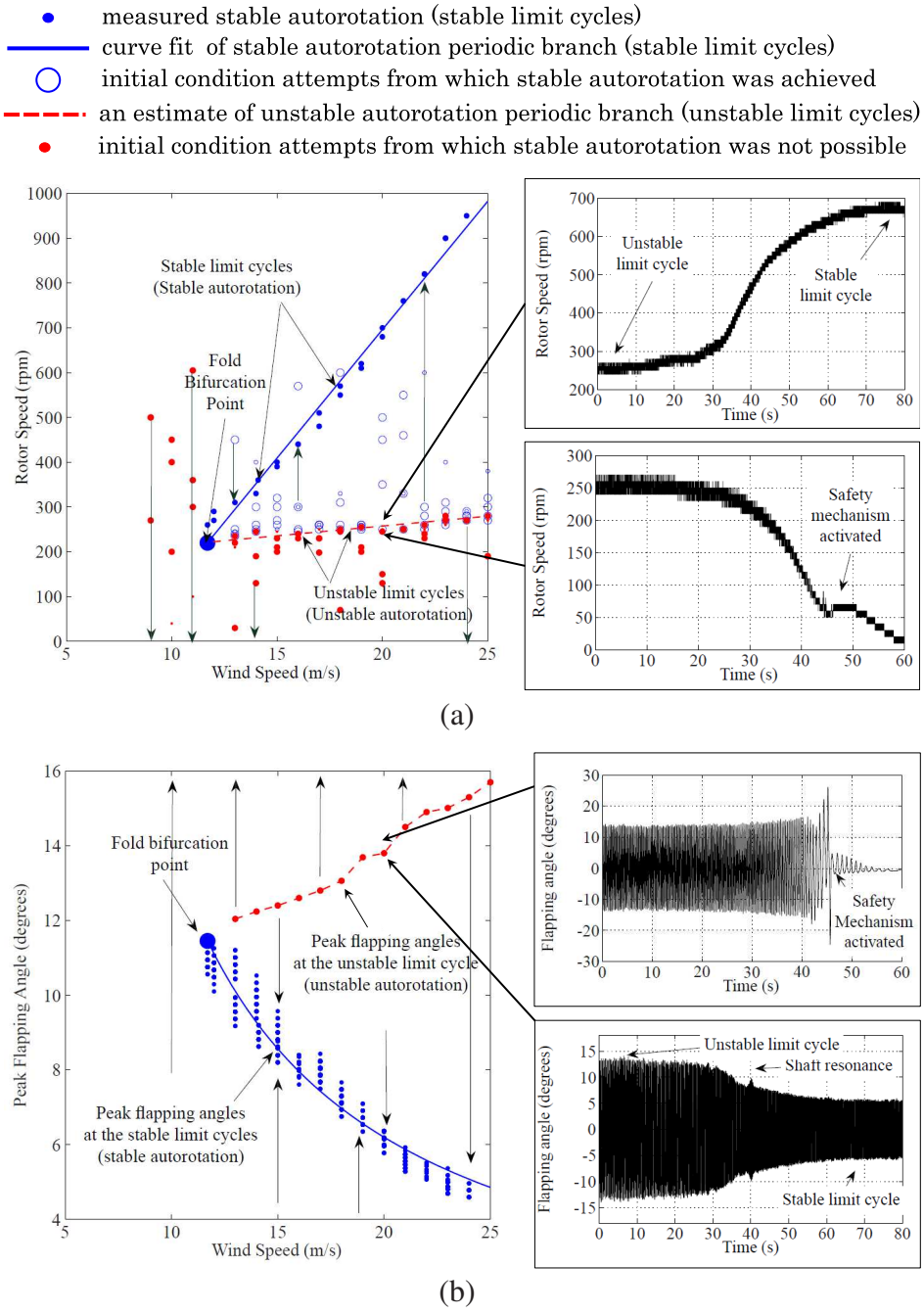

Fig. 8 Experimental bifurcation diagrams showing projections in (a) the rotational velocity and (b) the flapping angle for the autorotating rotor, $\theta_{shaft} = 7^\circ$ and $\theta_{col} = 1^\circ$. The arrows indicate the direction of the trajectories' transient behavior. Blade responses at wind speed U= 20 m/s for two close but different initial conditions are shown on the right.

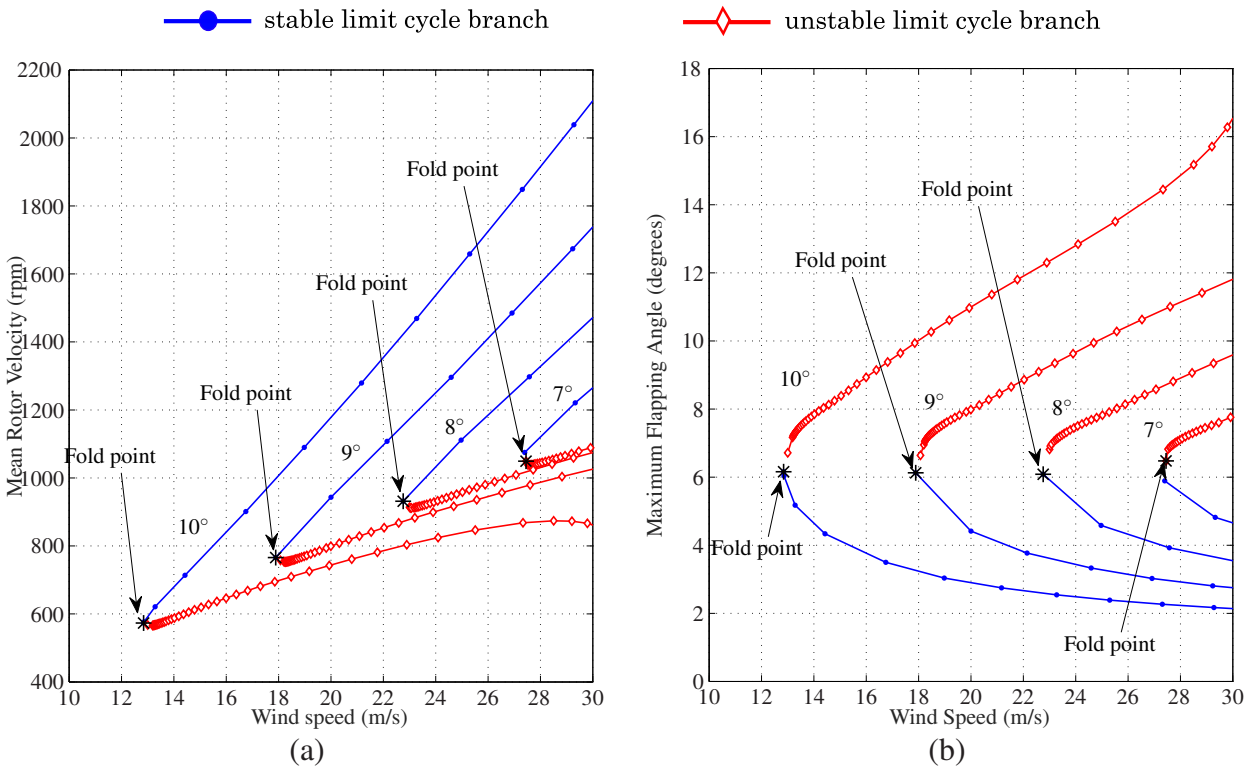

Fig. 9 Bifurcation diagrams for the numerical model showing projections in (a) rotor speed and (b) flapping angle, at shaft angles of 4° to 10° and a collective pitch angle $\theta_{col} = 1°$. The continuation parameter is the forward flow speed.

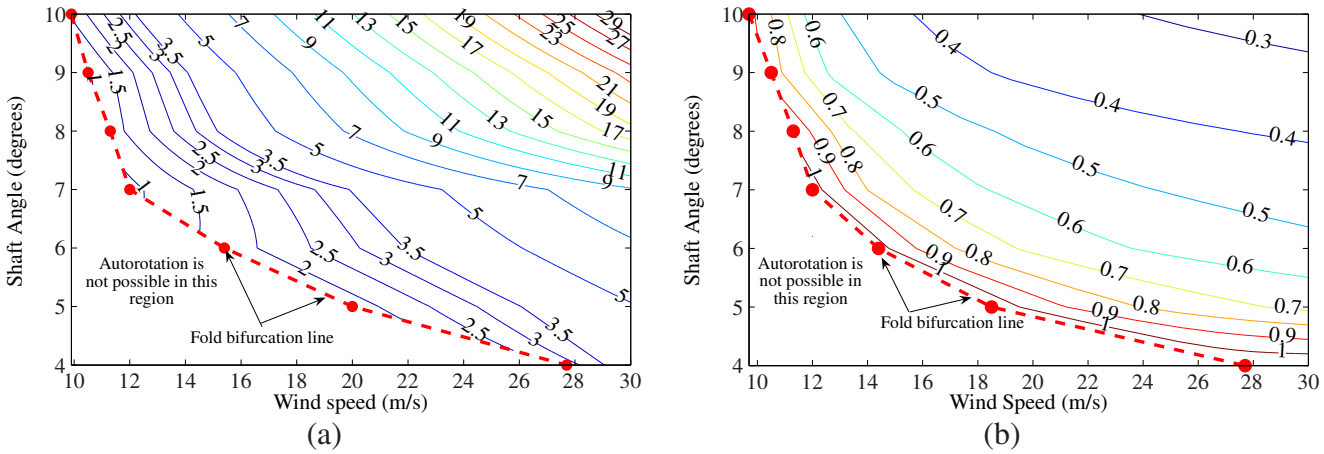

Fig. 10 Contour plots of (a) rotor lift in Newton and (b) advance ratio imposed on two-parameter experimental bifurcation diagrams with respect to wind speed and shaft angle, $\theta_{col} = 1^{\circ}$.

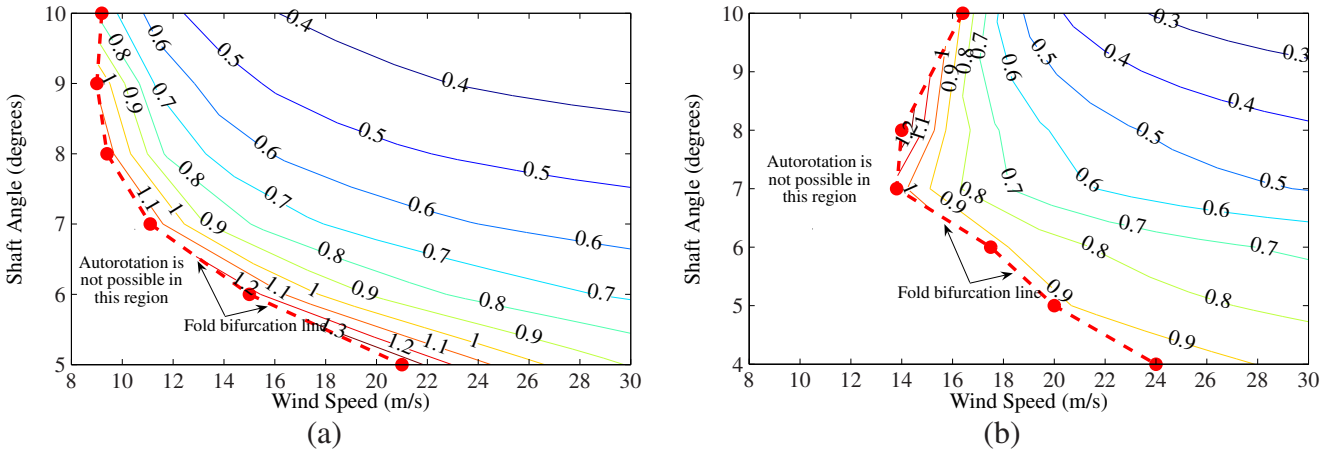

Fig. 11 Advance ratio contour plot imposed on an experimental bifurcation diagram with respect to wind speed and shaft angle at (a) $\theta_{col} = 0^\circ$ and (b) $\theta_{col} = 2^\circ$.

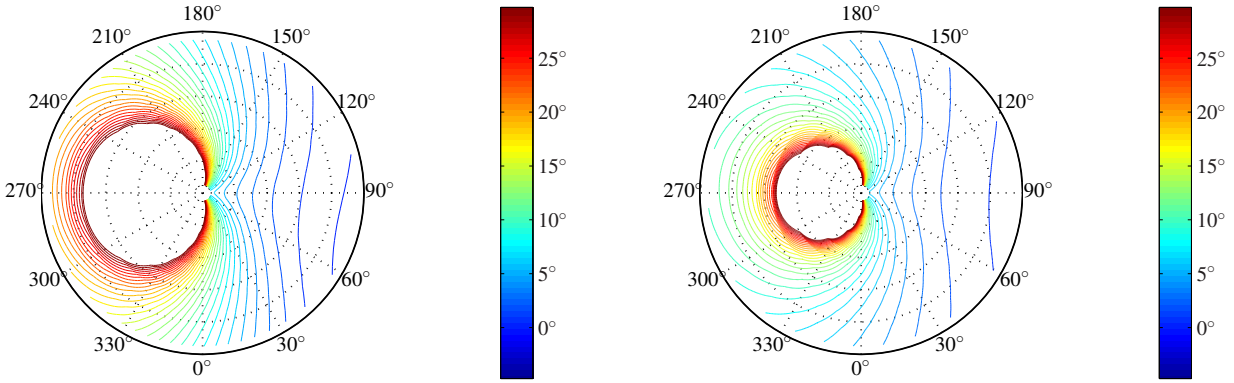

(a) $U = 27$ m/s (b) $U = 40$ m/s

Fig. 12 Distribution of angles of attack (degrees) using the numerical model across the rotor disc in stable autorotation, for (a) $U = 27$ m/s, close to the fold bifurcation point and for (b) $U = 40$ m/s, far from the bifurcation point. $\theta_{col} = 1^\circ$ and $\theta_{shaft} = 7^\circ$.

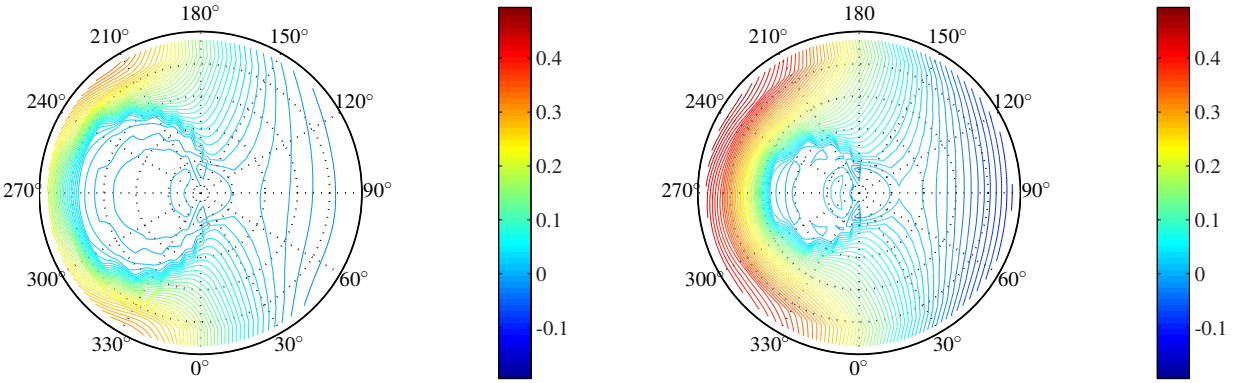

(a) $U = 27$ m/s (b) $U = 40$ m/s

Fig. 13 Distribution of elemental torque (Nm) using the numerical model across the rotor disc in stable autorotation, for (a) $U = 27$ m/s, close to the fold bifurcation point and for (b) $U = 40$ m/s, far from the bifurcation point. $\theta_{col} = 1^\circ$ and $\theta_{shaft} = 7^\circ$.

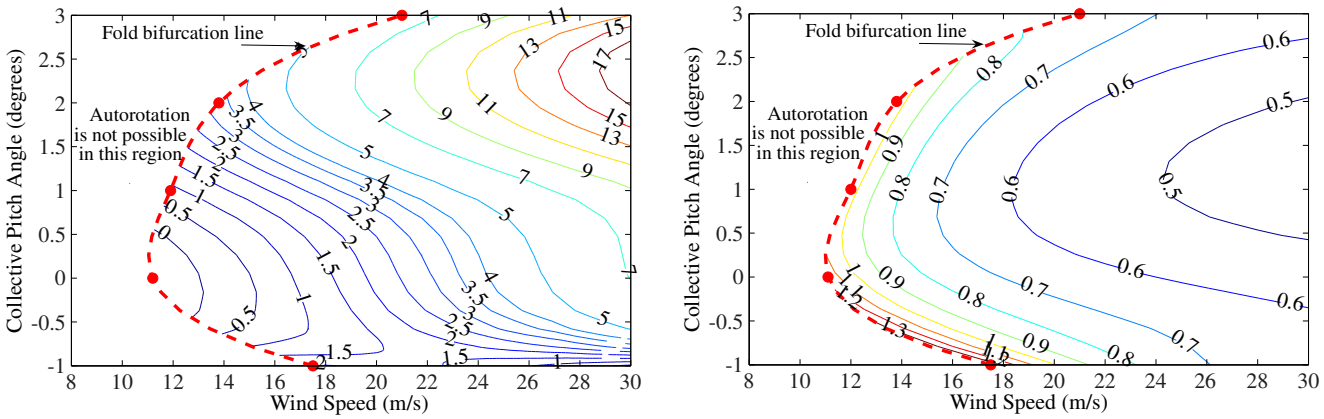

Fig. 14 Contour plots of (a) rotor lift in Newton (from Ref. 49) and (b) advance ratio imposed on a two-parameter experimental bifurcation diagram with respect to wind speed and collective pitch angle at $\theta_{shaft} = 7^{\circ}$.

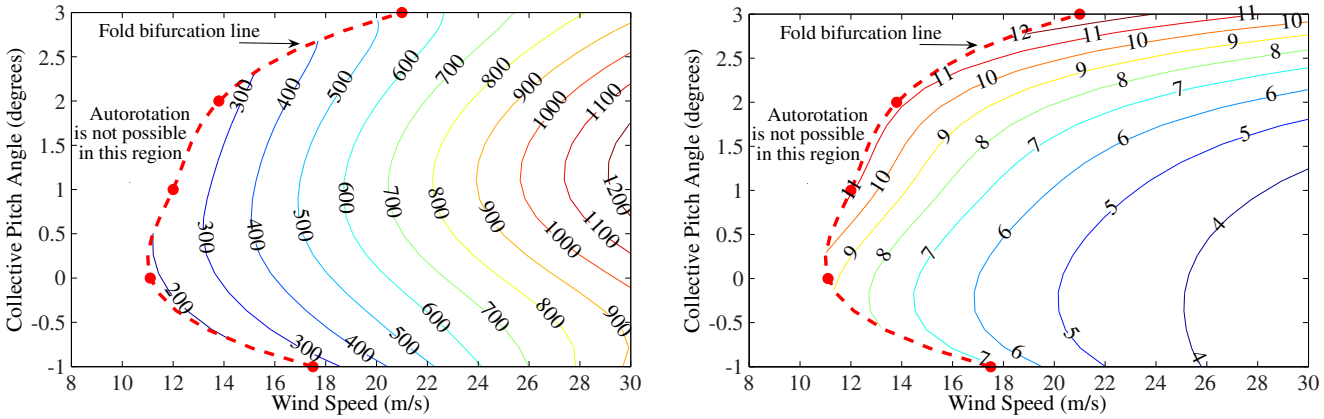

Fig. 15 Contour plots of (a) rotor speed in rpm and (b) blade peak flapping angle in degrees imposed on a two-parameter experimental bifurcation diagram with respect to wind speed and collective pitch angle at $\theta_{shaft} = 7^{\circ}$.

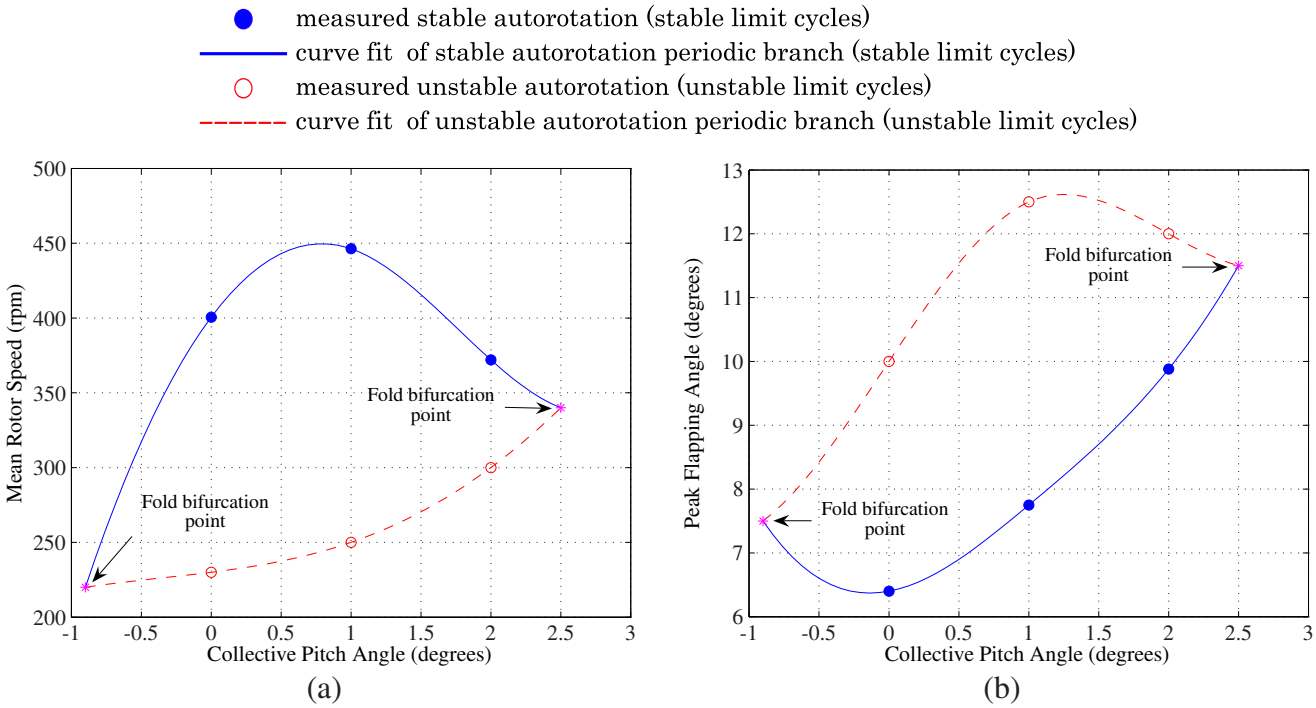

Fig. 16 Experimental bifurcation diagram showing projections in (a) rotational velocity and (b) flapping angle, for an autorotating rotor. θ_{col} is the continuation parameter, $\theta_{shaft} = 7^\circ$ and $U = 16$ m/s. From Ref. 49.

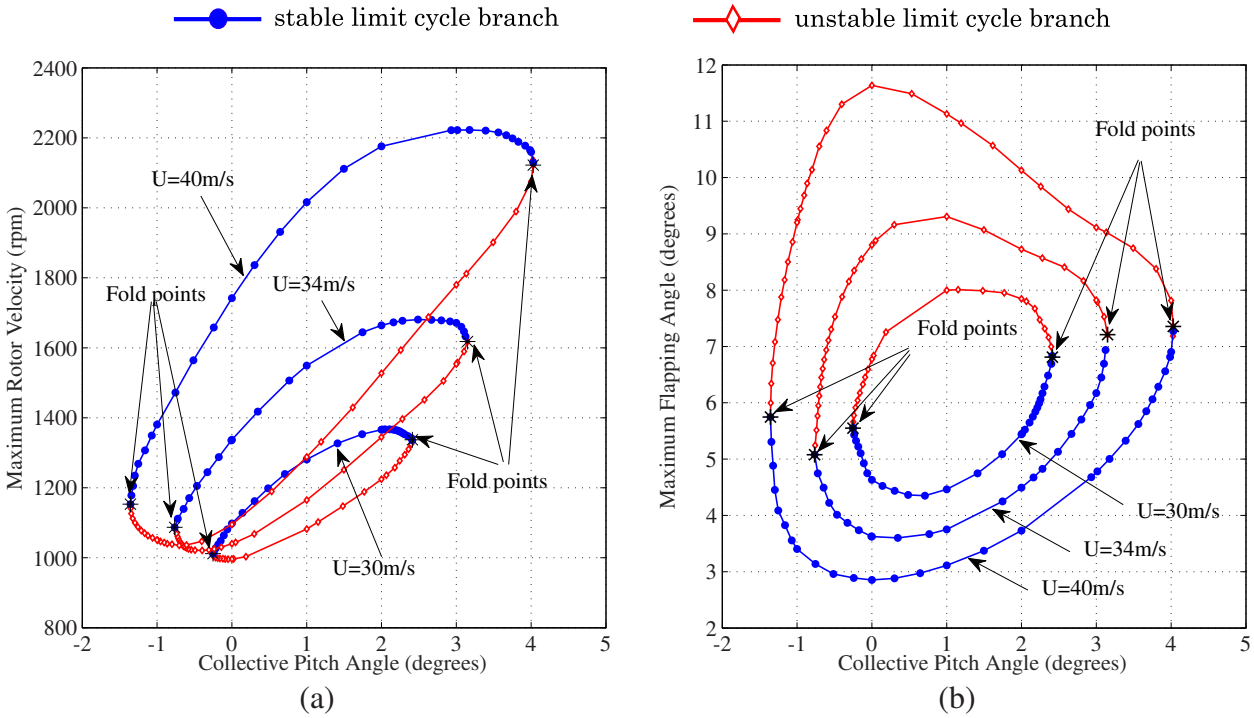

Fig. 17 Bifurcation diagrams for the numerical model showing projections in (a) rotor speed and (b) flapping angle, at flow speeds from 30 m/s to 40 m/s and shaft angle $\theta_{shaft} = 7°$. The continuation parameter is the collective pitch angle θ_{col}.

List of Tables

Table 1. Examples of autogyro accidents in the UK caused by rotor related instabilities.

Year	Autogyro	Cause of accident	Reference
1990	Air Command	Rotor speed lost in flight	(Ref. 78)
2003	Bensen	Control lost after rotor blades struck rudder in flight	(Ref. 79)
2006	RAF 2000 Autogyro	Main rotor struck vertical stabilizer, propeller and rudder in flight	(Ref. 80)

Table 2. Allocation of state values for the rotor blades

States as defined in the model	Corresponding states for blade 1	Corresponding states for blade 2
ψ	ψ	$\psi+\pi$
$\dot{\psi}$	$\dot{\psi}$	$\dot{\psi}$
β	β	$-\beta$
$\dot{\beta}$	$\dot{\beta}$	$-\dot{\beta}$